Gastroenterology 2018;■:1–16

Hdac1 Regulates Differentiation of Bipotent Liver Progenitor Cells During Regeneration Via Sox9b and Cdk8

Sungjin Ko,[1,2] Jacquelyn O. Russell,[2] Jianmin Tian,[2,3] Ce Gao,[4] Makoto Kobayashi,[5] Rilu Feng,[6] Xiaodong Yuan,[6] Chen Shao,[7] Huiguo Ding,[8] Minakshi Poddar,[2] Sucha Singh,[2] Joseph Locker,[2,3] Hong-Lei Weng,[6] Satdarshan P. Monga,[2,3,9] and Donghun Shin[1,3]

[1]Department of Developmental Biology, McGowan Institute for Regenerative Medicine, Pittsburgh, Pennsylvania; [2]Department of Pathology, McGowan Institute for Regenerative Medicine, Pittsburgh, Pennsylvania; [3]Pittsburgh Liver Research Center, McGowan Institute for Regenerative Medicine, Pittsburgh, Pennsylvania; [4]MOE Key Laboratory for Molecular Animal Nutrition, College of Animal Sciences, Zhejiang University, Hangzhou, China; [5]Department of Molecular and Developmental Biology, Faculty of Medicine, University of Tsukuba, Tsukuba, Japan; [6]Department of Medicine II, Section Molecular Hepatology, Medical Faculty Mannheim, Heidelberg University, Mannheim, Germany; [7]Department of Pathology, Beijing You'an Hospital, Capital Medical University, Beijing, China; [8]Department of Gastroenterology and Hepatology, Beijing You'an Hospital, Capital Medical University, Beijing, China and [9]Department of Medicine, University of Pittsburgh, Pittsburgh, Pennsylvania

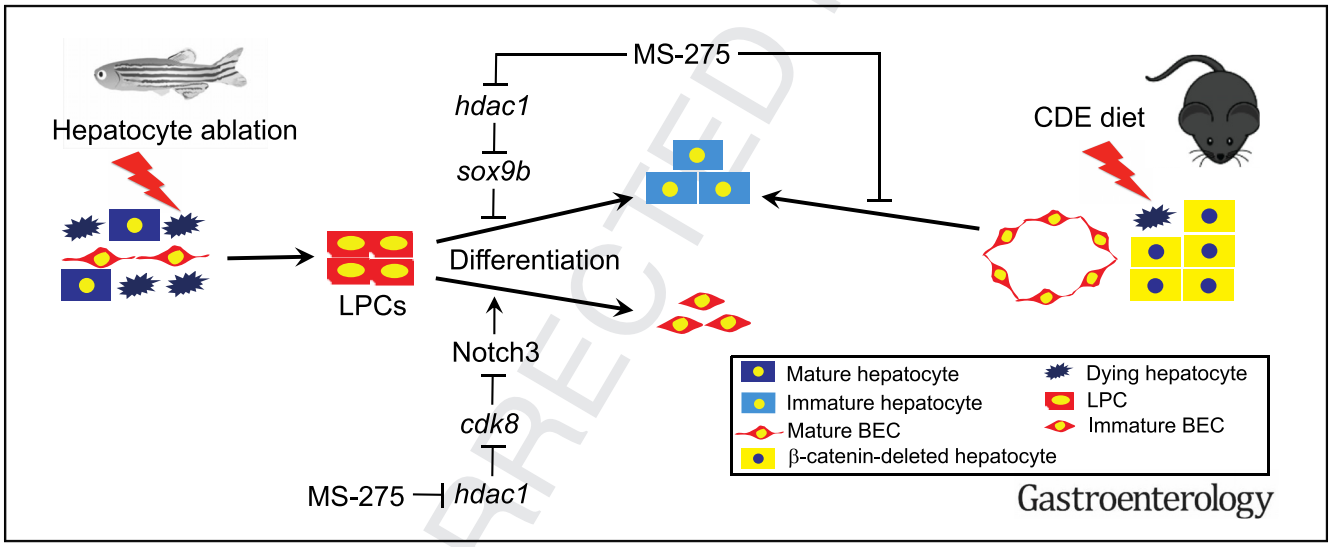

BACKGROUND & AIMS: Upon liver injury in which hepatocyte proliferation is compromised, liver progenitor cells (LPCs), derived from biliary epithelial cells (BECs), differentiate into hepatocytes. Little is known about the mechanisms of LPC differentiation. We used zebrafish and mouse models of liver injury to study the mechanisms. **METHODS:** We used transgenic zebrafish, Tg(*fabp10a:CFP-NTR*), to study the effects of compounds that alter epigenetic factors on BEC-mediated liver regeneration. We analyzed zebrafish with disruptions of the histone deacetylase 1 gene (*hdac1*) or exposed to MS-275 (an inhibitor of Hdac1, Hdac2, and Hdac3). We also analyzed zebrafish with mutations in *sox9b*, *fbxw7*, *kdm1a*, and *notch3*. Zebrafish larvae were collected and analyzed by whole-mount immunostaining and in situ hybridization; their liver tissues were collected for quantitative reverse transcription polymerase chain reaction. We studied mice in which hepatocyte-specific deletion of β-catenin ($Ctnnb1^{flox/flox}$ mice injected with AAV8-TBG-Cre) induces differentiation of LPCs into hepatocytes after a choline-deficient, ethionine-supplemented (CDE) diet. Liver tissues were collected and analyzed by immunohistochemistry and immunoblots. We performed immunohistochemical analyses of liver tissues from patients with compensated or decompensated cirrhosis or acute on chronic liver failure (n = 15). **RESULTS:** Loss of Hdac1 activity in zebrafish blocked differentiation of LPCs into hepatocytes by increasing levels of *sox9b* mRNA and reduced differentiation of LPCs into BECs by increasing levels of *cdk8* mRNA, which encodes a negative regulator gene of Notch signaling. We identified Notch3 as the receptor that regulates differentiation of LPCs into BECs. Loss of activity of Kdm1a, a lysine demethylase that forms repressive complexes with Hdac1, produced the same defects in differentiation of LPCs into hepatocytes and BECs as observed in zebrafish with loss of Hdac1 activity. Administration of MS-275 to mice with hepatocyte-specific loss of β-catenin impaired differentiation of LPCs into hepatocytes after the CDE diet. HDAC1 was expressed in reactive ducts and

hepatocyte buds of liver tissues from patients with cirrhosis. **CONCLUSIONS:** Hdac1 regulates differentiation of LPCs into hepatocytes via Sox9b and differentiation of LPCs into BECs via Cdk8, Fbxw7, and Notch3 in zebrafish with severe hepatocyte loss. HDAC1 activity was also required for differentiation of LPCs into hepatocytes in mice with liver injury after the CDE diet. These pathways might be manipulated to induce LPC differentiation for treatment of patients with advanced liver diseases.

Keywords: Hepatic; Development; CDE Diet; Signal Transduction.

Upon liver injury, hepatocytes proliferate to recover lost liver mass. However, when hepatocyte proliferation is compromised, a phenomenon observed in advanced liver diseases, biliary epithelial cells (BECs) activate or dedifferentiate into liver progenitor cells (LPCs), also called *oval cells* or *ductular reactions*, and then differentiate into hepatocytes.[1,2] A correlation between disease severity and LPC number in patients with chronic liver diseases[3] suggests that BECs are indeed activated in the diseased liver but that the activated LPCs poorly differentiate into hepatocytes. Although LPCs can give rise to hepatocytes, they also secrete inflammatory cytokines that can cause inflammation and subsequent fibrosis.[4] Therefore, it has been hypothesized that promoting differentiation of LPCs into hepatocytes has a 2-fold beneficial effect in liver patients: generating more hepatocytes and reducing inflammation. Despite the potential clinical significance of the mechanistic understanding of LPC differentiation, the molecular mechanisms underlying this process are poorly understood.

We[5] and others[6,7] previously reported that after near-complete hepatocyte ablation in zebrafish, BECs extensively contribute to hepatocytes, thereby leading to a full liver recovery. Recently, a similar BEC-driven liver regeneration was observed in mice in the settings of impaired hepatocyte proliferation[8,9] and long-term chronic injury.[10] In human regressed cirrhotic livers, a large percentage of parenchyma appears to originate from LPCs,[11] implying the importance of BEC-driven liver regeneration in cirrhosis regression. Given the robust BEC-driven liver regeneration in these zebrafish and mouse liver injury models, these models will help elucidate the molecular mechanisms underlying liver regeneration in advanced liver diseases (i.e., LPC-driven liver regeneration).

In the zebrafish model, the complete ablation of hepatocytes in larvae leads to the collapse of the entire intrahepatic biliary network, and all preexisting BECs dedifferentiate into LPCs.[12] During regeneration, a small subset of LPCs differentiate into BECs, with which the intrahepatic biliary network is reestablished. Thus, this zebrafish model will allows investigation into the differentiation of LPCs into BECs and hepatocytes. Given the contribution of LPCs differentiated into BECs in rodent[13] and human[14] biliary injury settings, understanding the mechanisms underlying LPC differentiation into BECs and hepatocytes will lead to the comprehensive understanding of the molecular mechanisms underlying LPC-driven liver regeneration. Given the key roles of epigenetics in cellular reprogramming,[15] we focused on epigenetic regulators that can control LPC differentiation, because promoting its differentiation may have a beneficial effect on patients with advanced liver diseases. Here, we show the crucial role of the histone deacetylase Hdac1 in the differentiation of LPCs into both hepatocytes and BECs and provide 2 distinct, novel molecular mechanisms by which Hdac1 regulates this differentiation process during regeneration.

WHAT YOU NEED TO KNOW

BACKGROUND AND CONTEXT

Placeholder text • Placeholder text • Placeholder text • Placeholder text • Placeholder text • Placeholder text • Placeholder text • Placeholder text • Placeholder text • Placeholder text •

NEW FINDINGS

Placeholder text • Placeholder text • Placeholder text • Placeholder text • Placeholder text • Placeholder text • Placeholder text • Placeholder text • Placeholder text • Placeholder text •

LIMITATIONS

Placeholder text • Placeholder text • Placeholder text • Placeholder text • Placeholder text • Placeholder text • Placeholder text • Placeholder text • Placeholder text • Placeholder text •

IMPACT

Placeholder text • Placeholder text • Placeholder text • Placeholder text • Placeholder text • Placeholder text • Placeholder text • Placeholder text • Placeholder text • Placeholder text •

Materials and Methods

Zebrafish and Mouse Studies

All animals are housed in temperature- and light-controlled facilities and are maintained in accordance with the Guide for Care and Use of Laboratory Animals and the Animal Welfare Act. Experiments were performed with approval of the Institutional Animal Care and Use Committee at the University of Pittsburgh. Zebrafish and mouse lines used in this work, detailed analytic methods, and human studies are described in the supplementary material.

Abbreviations used in this paper: **A, ablation; ACLF, acute-on-chronic liver failure; BEC, biliary epithelial cell; CDE, choline-deficient, ethionine supplemented; CFP, cyan fluorescent protein; ChIP, chromatin immunoprecipitation; DMSO, dimethyl sulfoxide; dpf, days postfertilization; GFP, green fluorescent protein; H2B, histone 2B; HBV, hepatitis B virus; H3K9ac, acetylation of histone H3 at lysine 9; kb, kilo base; LPC, liver progenitor cell; Mtz, metronidazole; NICD, Notch intracellular domain; qPCR, quantitative polymerase chain reaction; R, regeneration.**

0016-5085/$36.00
https://doi.org/10.1053/j.gastro.2018.09.039

Results

Identification of Small Molecules That Block LPC-to-Hepatocyte Differentiation During Regeneration

To identify chemical agents that affect LPC-to-hepatocyte differentiation, we performed an in vivo chemical screening using our established zebrafish model of BEC-driven liver regeneration.[5] A library of known epigenetic compounds was selected, because our previous chemical screening resulted in the identification of BET proteins as important regulators of BEC-driven liver regeneration,[12] raising a possibility that other epigenetic regulators may also play essential roles in this process. For this screening, we used triple transgenic zebrafish: 1) *Tg(fabp10a:CFP-NTR)*, which expresses nitroreductase fused with cyan fluorescent protein (CFP) in hepatocytes, allowing for hepatocyte-specific ablation upon metronidazole (Mtz) treatment; 2) *Tg(Tp1:H2B-mCherry)*, which expresses histone 2B (H2B) and mCherry fusion proteins strongly in BECs and weakly in BEC-derived hepatocytes; and 3) *Tg(fabp10a:rasGFP)*, which expresses the membrane form of green fluorescent protein (GFP) strongly in hepatocytes and weakly in LPCs.[12] The Q11 triple transgenic larvae were treated with Mtz from 3.5 to 5 days postfertilization (dpf) for 36 hours (ablation, A36h), which resulted in near-complete hepatocyte ablation, followed by Mtz washout, scored as the start of regeneration (regeneration, R0h). We treated the larvae with compounds from A20h, before BEC dedifferentiation occurs, to R24h, at which point larvae were harvested for subsequent whole-mount immunostaining (Figure 1*A*). To identify a compound that regulates LPC-to-hepatocyte differentiation, we examined the expression of a hepatocyte marker, Bhmt.[16] Through this screening, we identified 3 compounds that blocked Bhmt expression in regenerating livers at R24h: MS-275, trichostatin A, and OG-L002 (Figure 1*B*). In Q12 regenerating livers treated with these 3 compounds, *fabp10a:*rasGFP expression was still detected, although lower than in control regenerating livers (Figure 1*B*), suggesting that BECs dedifferentiated into LPCs in these compound-

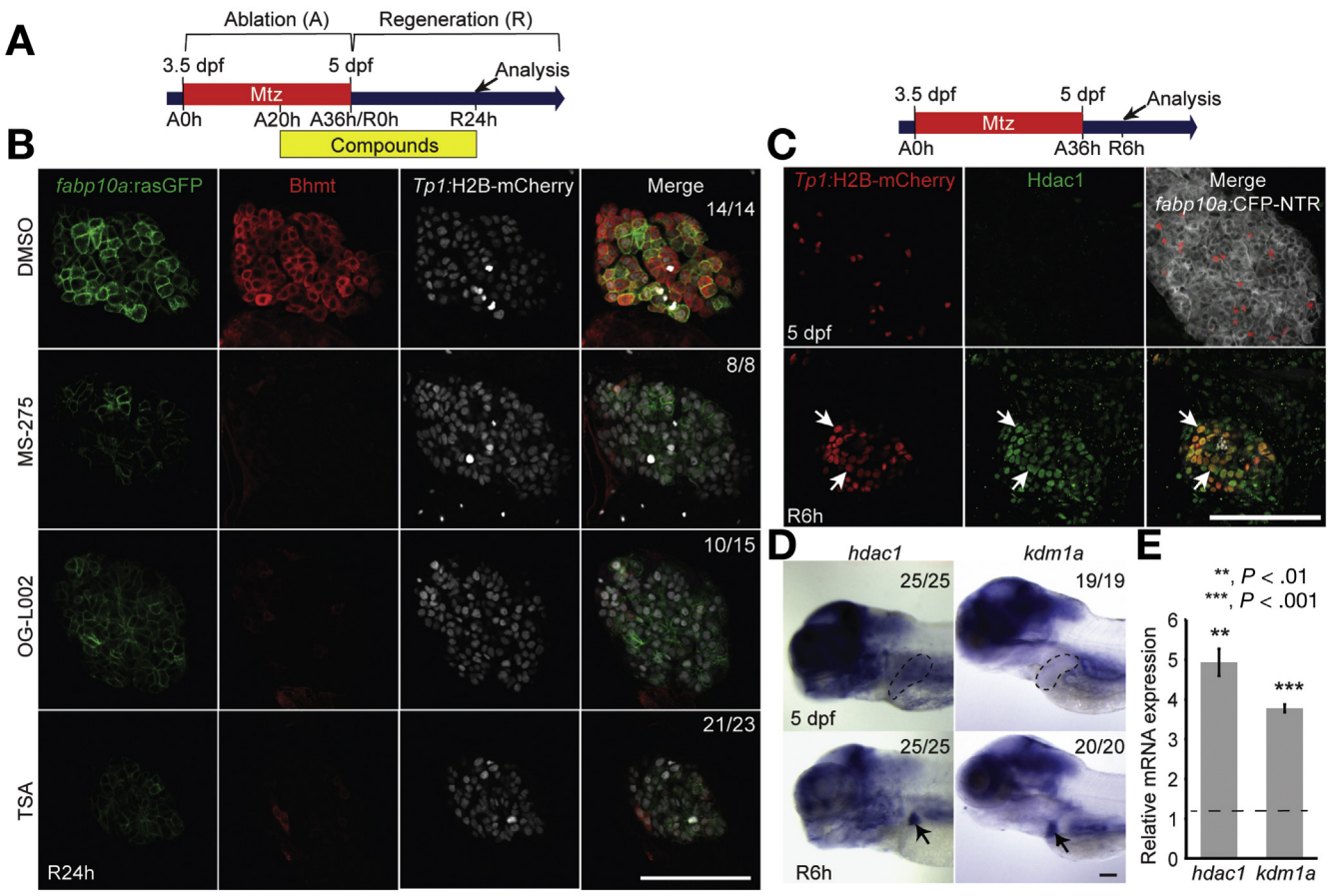

Figure 1. Identification of compounds that block LPC-to-hepatocyte differentiation during regeneration. (*A*) Experimental scheme illustrating the stages of Mtz and testing compound treatment and analysis (*arrow*). (*B*) Single-optical section images showing the expression of Bhmt, *fabp10a:*rasGFP, and *Tp1:*H2B-mCherry in regenerating livers at R24h. Numbers indicate the proportion of larvae exhibiting the representative expression shown. (*C*) Single-optical section images showing the expression of Hdac1, *Tp1:*H2B-mCherry, and *fabp10a:*CFP-NTR in normal liver at 5 dpf and regenerating liver at R6h. Arrows point to BEC-derived cells expressing Hdac1. (*D*) Whole-mount in situ hybridization (WISH) images showing *hdac1* and *kdm1a* expression in normal livers at 5 dpf and regenerating livers at R6h. Dashed lines outline control livers; arrows point to regenerating livers. (*E*) qPCR data showing the relative expression levels of *hdac1* and *kdm1a* between 5-dpf control livers and R6h regenerating livers. Scale bars, 100 μm; error bars show ± standard error of the mean. Q24

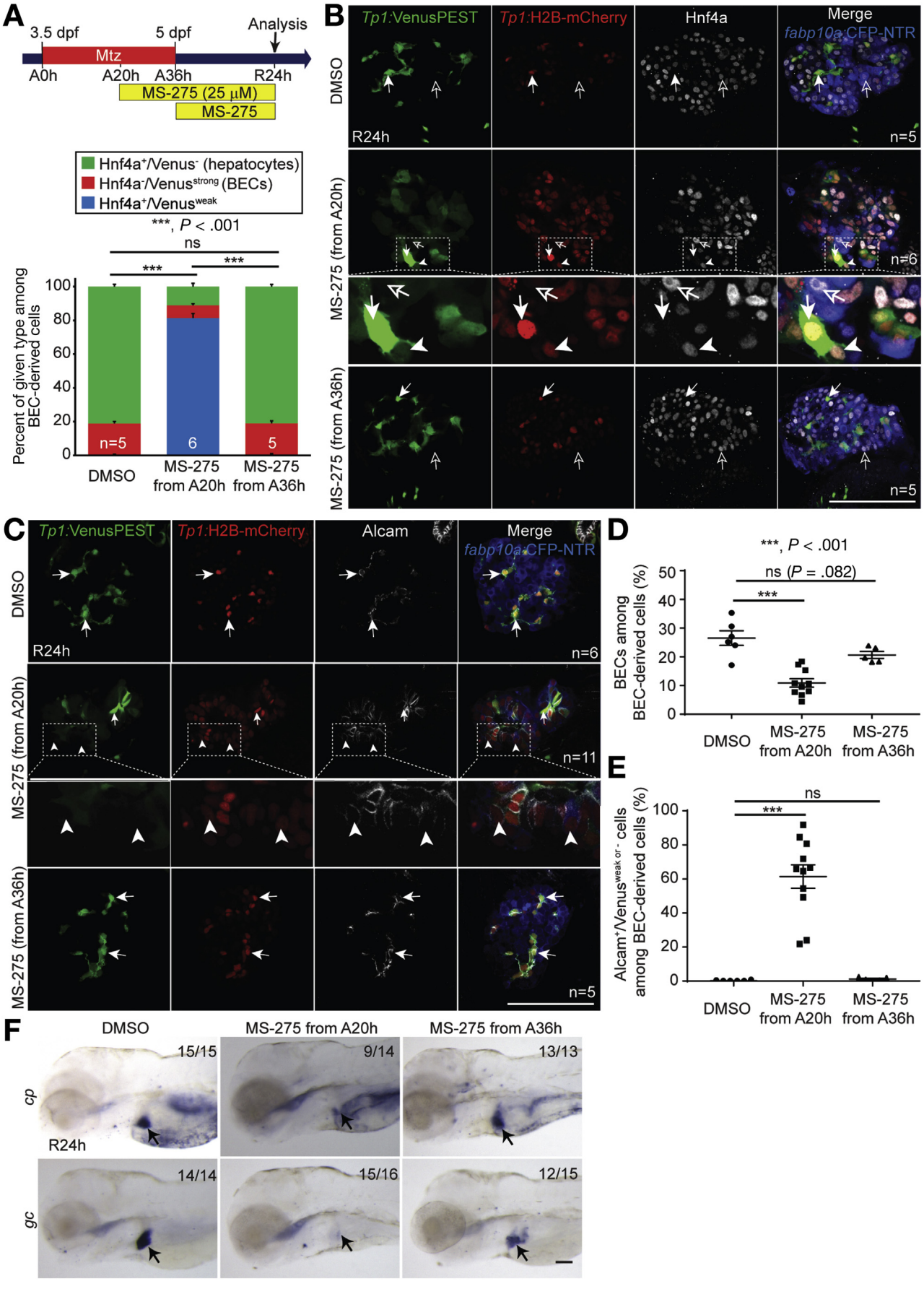
A
3.5 dpf
5 dpf
Analysis
Mtz
A0h
A20h
A36h
R24h
MS-275 (25 μM)
MS-275
Hnf4a+/Venus- (hepatocytes)
Hnf4a-/Venusstrong (BECs)
Hnf4a+/Venusweak
***, P < .001
ns
***
***
Percent of given type among BEC-derived cells
100
80
60
40
20
0
n=5
6
5
DMSO
MS-275 from A20h
MS-275 from A36h
B
Tp1:VenusPEST
Tp1:H2B-mCherry
Hnf4a
Merge
fabp10a:CFP-NTR
DMSO
R24h
n=5
MS-275 (from A20h)
n=6
MS-275 (from A36h)
n=5
C
Tp1:VenusPEST
Tp1:H2B-mCherry
Alcam
Merge
fabp10a:CFP-NTR
DMSO
R24h
n=6
MS-275 (from A20h)
n=11
MS-275 (from A36h)
n=5
D
***, P < .001
ns (P = .082)
***
BECs among BEC-derived cells (%)
50
40
30
20
10
0
DMSO
MS-275 from A20h
MS-275 from A36h
E
ns
***
Alcam+/Venusweak or - cells among BEC-derived cells (%)
100
80
60
40
20
0
DMSO
MS-275 from A20h
MS-275 from A36h
F
DMSO
MS-275 from A20h
MS-275 from A36h
cp
R24h
15/15
9/14
13/13
gc
14/14
15/16
12/15

treated regenerating livers. MS-275 inhibits HDAC1/2/3,[17,18] and trichostatin A is a pan-HDAC inhibitor.[19] OG-L002 inhibits lysine-specific histone demethylases 1A (KDM1A, also called LSD1),[20] which forms the CoREST repressor complex with HDAC1/2.[21] The identification of these compounds suggests that HDAC1/2-containing, histone-modifying repressor complexes regulate LPC-to-hepatocyte differentiation during regeneration. Moreover, we found that *hdac1* and *kdm1a* expressions were highly up-regulated in regenerating livers at R6h (Figure 1*C–E*) and diminished later at R12h and R24h (Supplementary Figure 1). Specifically, Hdac1 expression in BECs was not yet observed at A18h but was strongly induced at R6h; as the liver recovered, its expression was reduced at R24h (Supplementary Figure 1*A*, *arrows*). Collectively, given the absence of the *hdac2* gene in the zebrafish genome, we hypothesized that *hdac1* regulates LPC-to-hepatocyte differentiation during regeneration.

MS-275 Treatment Impairs LPC Differentiation Into Either Hepatocytes or BECs

We next investigated in detail the effect of MS-275 treatment on BEC-driven liver regeneration by examining the expression of additional liver markers at R24h (Figure 2*A*). During BEC-driven liver regeneration, Hnf4a, a hepatoblast/hepatocyte marker, expression is induced in LPCs and is maintained in hepatocytes but not in BECs; BEC marker expression is sustained in LPCs but disappears from LPCs when these cells differentiate into hepatocytes.[5] In MS-275–treated regenerating livers, Hnf4a was normally induced in BEC-derived cells (Figure 2*B*), further supporting the normal dedifferentiation of BECs into LPCs. *Tg(Tp1:VenusPEST)* and *Tg(Tp1:H2B-mCherry)* lines express fluorescent proteins under the same *Tp1* promoter containing the Notch-responsive element[22] and show BECs in the liver.[23] The short half-life of VenusPEST proteins shows only cells with active Notch signaling, whereas the prolonged stability of H2B-mCherry proteins allows for tracing of BEC-derived cells even when Notch signaling is off.[5] Analysis of these BEC markers together with Hnf4a showed the reduced number of hepatocytes (Hnf4a$^+$/VenusPEST$^-$) and BECs (Hnf4a$^-$/VenusPEST^{strong}) in MS-275–treated regenerating livers at R24h compared with controls (Figure 2*B–D*). Undifferentiated or less-differentiated cells, defined as Hnf4a$^+$/VenusPEST^{weak}, were detected in MS-275–treated, but not control, regenerating livers (Figure 2*B*, blue bar), which was further confirmed by analyzing the expression of Alcam, another BEC marker. BECs are Alcam$^+$/VenusPEST^{strong} (Figure 2*C*, *arrows*), and hepatocytes are Alcam$^-$/VenusPEST$^-$. Alcam$^+$/VenusPEST$^{weak\ or\ -}$ cells (Figure 2*C*, *arrowheads*) were not detected in control regenerating livers, whereas these cells were abundantly present in MS-275–treated regenerating livers (Figure 2). The defect in LPC-to-hepatocyte differentiation was further confirmed by almost no expression of the hepatocyte markers *cp* and *gc* in MS-275–treated regenerating livers at R24h (Figure 2*F*). Moreover, the continuous treatment of MS-275 until R48h also blocked Bhmt expression in regenerating livers at R48h (Supplementary Figure 2*A*). However, the washout of MS-275 at A36h/R0h resulted in Bhmt expression in most regenerating livers at R24h, although weaker than in controls (Supplementary Figure 2*B*). MS-275 treatment from A36h did not affect LPC differentiation into either hepatocytes or BECs (Figure 2), indicating the A20h–A36h period as the critical time window of MS-275 effect on LPC differentiation during regeneration.

Upon 70% partial hepatectomy or carbon tetrachloride injection, in which hepatocytes contribute to regenerated hepatocytes (ie, hepatocyte-driven liver regeneration), hepatocyte-specific *Hdac1/2* double-knockout mice exhibit reduced hepatocyte proliferation and increased apoptosis.[24] Given this positive role of HDAC1/2 in hepatocyte-driven liver regeneration, we also examined the effect of MS-275 on proliferation and cell death during BEC-driven liver regeneration. The proliferation of BEC-derived cells was not significantly different between control and MS-275–treated regenerating livers at R6h (Supplementary Figure 3*A*) and R24h (Supplementary Figure 3*D*), and their number was comparable between dimethyl sulfoxide (DMSO)– and MS-275–treated regenerating livers at R0h (Supplementary Figure 3*G*). Unexpectedly, BEC proliferation, as assessed by the percentage of 5-ethynyl-2′-deoxyuridine$^+$ cells among BECs, was significantly increased in MS-275–treated regenerating livers at R24h compared with controls (Supplementary Figure 3*E*). Few BEC-derived cells were dying in either control or MS-275–treated regenerating livers at R12h (Supplementary Figure 3*F*). These proliferation and cell death data suggest a distinct role of Hdac1 in BEC-driven liver regeneration compared with hepatocyte-driven liver regeneration.

Figure 2. MS-275 treatment impairs LPC differentiation into either hepatocytes or BECs during regeneration. (*A*) Experimental scheme illustrating the stages of Mtz and MS-275 treatment and analysis (*arrow*). (*B*) Single-optical section images showing the expression of Hnf4a, *Tp1:*VenusPEST, *Tp1:*H2B-mCherry, and *fabp10a:*CFP-NTR in regenerating livers at R24h. Among BEC-derived, H2B-mCherry$^+$ cells, Hnf4a$^-$/VenusPEST^{strong} cells are BECs (arrows) and Hnf4a$^+$/VenusPEST$^-$ cells are hepatocytes (*open arrows*). A third cell type, Hnf4a$^+$/VenusPEST^{weak} cells, is present (*arrowheads*) in MS-275–treated but not control regenerating livers. Quantification of the percentage of hepatocytes, BECs, and undifferentiated or less-differentiated cells among H2B-mCherry$^+$ cells is shown; n indicates the number of larvae examined. (*C*) Single-optical section images showing the expression of Alcam, *Tp1:*VenusPEST, *Tp1:*H2B-mCherry, and *fabp10a:*CFP-NTR in regenerating livers at R24h. Arrows point to BECs; arrowheads point to Alcam$^+$/VenusPEST$^-$ cells derived from BECs. (*D*, *E*) Quantification of the percentage of (*D*) BECs or (*E*) Alcam$^+$/VenusPEST$^{weak\ or\ -}$ cells among H2B-mCherry$^+$ (BEC-derived) cells, as shown in *C*. (*F*) WISH images showing *cp* and *gc* expression in regenerating livers at R24h. Arrows point to regenerating livers. Numbers indicate the proportion of larvae exhibiting the representative expression shown. Scale bars, 100 μm; error bars show ± standard error of the mean. M, mol/L; WISH, whole-mount in situ hybridization.

Hdac1 Is Required for LPC Differentiation During BEC-Driven Liver Regeneration

HDAC1 and HDAC2 usually play redundant roles in mice; therefore, only deletion of both genes causes defects in diverse developmental or regeneration processes.[24,25] However, the absence of the *hdac2* gene in the zebrafish genome makes it possible to detect a phenotype in *hdac1*-mutant zebrafish.[26] The *hdac1* homozygous mutants die around 2–4 dpf and exhibit severe defects in multiple organs, including the liver, but heterozygous mutants normally survive without any noticeable defects.[26] Thus, we used *hdac1*$^{+/-}$ mutants for our BEC-driven liver regeneration study. BEC-driven liver regeneration appeared normal at R24h in *hdac1*$^{+/-}$ mutants; however, by reducing the dosage of MS-275 from 25 μmol/L, we found a dosage that resulted in a regeneration defect in only *hdac1*$^{+/-}$ but not wild-type larvae. The treatment of 10 μmol/L MS-275 blocked LPC-to-hepatocyte differentiation in *hdac1*$^{+/-}$ but not wild-type larvae, as assessed by Bhmt, *cp*, and *gc* expressions at R24h (Figure 3*A*–*D*). Although 10 μmol/L MS-275 treatment resulted in reduced BEC numbers in wild-type regenerating livers, the number was further decreased in *hdac1*$^{+/-}$ regenerating livers (Figure 3*E* and *F*). Altogether, these mutant data indicate *hdac1* as the key *hdac* gene required for LPC differentiation during regeneration.

Hdac1 Regulates LPC-to-Hepatocyte Differentiation by Repressing sox9b Expression

Given that genes and pathways used during development are often reused during regeneration, to determine the molecular mechanisms by which Hdac1 regulates LPC differentiation, we examined the expression levels of hepatic genes that play important roles in liver development. Quantitative polymerase chain reaction (qPCR) analysis showed that *sox9b* and *foxa3* were highly up-regulated in MS-275–treated regenerating livers compared with DMSO-treated regenerating livers at R6h (Figure 4*A*). We focused on these genes because both Hdac1 and Kdm1a inhibition impaired LPC-driven liver regeneration (Figure 1*B*), suggesting that the CoREST complex, which contains Hdac1 and Kdm1a, controls the regeneration by repressing gene expression. It was reported that HDAC inhibitor treatment increased *SOX9* expression in human primary fetal hepatocytes[27] and clear-cell sarcoma cells.[28] Trichostatin A treatment or *HDAC1* knockdown also increased *SOX9* expression in human lung adenocarcinoma cells.[29] Given the role of SOX9 in maintaining stem cell/progenitor states in liver cancer[30] and mammary[31] stem cells, we hypothesized that the enhanced *sox9b* expression in MS-275–treated regenerating livers prevented LPC differentiation. To test this hypothesis, we lowered *sox9b* expression in regenerating livers using *sox9b* heterozygous mutants. As previously reported, BEC-driven liver regeneration failed to occur in *sox9b*$^{-/-}$ mutants,[7] whereas it did occur in *sox9b*$^{+/-}$ mutants (Supplementary Figure 4). In *sox9b*$^{+/-}$ larvae, Bhmt was normally expressed in regenerating hepatocytes at R24h (Supplementary Figure 4*A*), but number of BECs was significantly reduced at this stage compared with their wild-type siblings (Supplementary Figure 4*B*), indicating the haploinsufficiency of *sox9b* in regulating BEC number during BEC-driven liver regeneration. The hepatocyte differentiation defect observed in *hdac1*$^{+/-}$ larvae treated with 10 μmol/L MS-275 was significantly rescued in *sox9b*$^{+/-}$ mutants, as assessed by Bhmt expression (Figure 4*B*). In contrast to this hepatocyte differentiation defect, the reduced BEC number phenotype was not rescued in *sox9b*$^{+/-}$ mutants (Supplementary Figure 4*C*).

Next, using a chromatin immunoprecipitation (ChIP)-qPCR assay, we determined whether the enhanced *sox9b* expression in MS-275–treated regenerating livers is mediated by the hyperacetylation of the *sox9b* genomic locus. To obtain the amount of liver tissues required for this assay, we used adult zebrafish, as previously reported.[5] The *Tg (fabp10a:CFP-NTR)* adult fish were treated with 5 mmol/L Mtz only for 5 hours and subsequently treated with MS-275 from R19h to R4d. As observed in the larvae, Bhmt expression was greatly reduced and *sox9b* expression was significantly up-regulated in MS-275–treated regenerating adult livers compared with control regenerating livers (Figure 4*C* and *D*), suggesting an LPC-to-hepatocyte differentiation defect. To examine the histone acetylation status of the *sox9b* genomic locus, we assessed the levels of acetylation of histone H3 at lysine 9 (H3K9ac), a marker of active gene promoters, within the 3-kilobase (kb) region from the *sox9b* transcription start site, because such a 3-kb region regulates *Sox9* expression in the mouse liver[32] and zebrafish.[33] We randomly selected 14 genomic loci in this region and further narrowed this down to 2 loci for H3K9ac enrichment analysis. We also selected a region that is located 8.5 kb upstream from the *sox9b* 5′ untranslated region as a negative control. H3K9ac enrichment in the 2 selected regions was significantly increased in regenerating livers compared with uninjured livers (Figure 4*E*), consistent with the enhanced expression of *sox9b* in regenerating livers (Figure 4*D*). The H3K9ac enrichment was further increased in MS-275–treated regenerating livers compared with the control regenerating livers (Figure 4*E*). As a negative control, the level of H3K9ac enrichment in the control region was very low and comparable between the uninjured livers and MS-275–treated regenerating livers (Figure 4*E*). Altogether, these *sox9b* mutant and ChIP-qPCR data show *sox9b* as the key downstream target gene of Hdac1 that regulates LPC-to-hepatocyte differentiation.

Hdac1 Regulates LPC-to-BEC Differentiation by Repressing Cdk8/Fbxw7-Mediated Degradation of Notch Intracellular Domain

We next sought to determine the molecular mechanism by which Hdac1 regulates LPC-to-BEC differentiation. During development, Notch signaling is required for differentiation of hepatoblasts into BECs; overactivation of Notch signaling in hepatoblasts makes excessive BECs.[32] Furthermore, Notch signaling has been considered a key driver that differentiates LPCs into BECs in rodent biliary injury models[13] and human biliary diseases.[14] Thus, we hypothesized that the defect in LPC-to-BEC differentiation observed

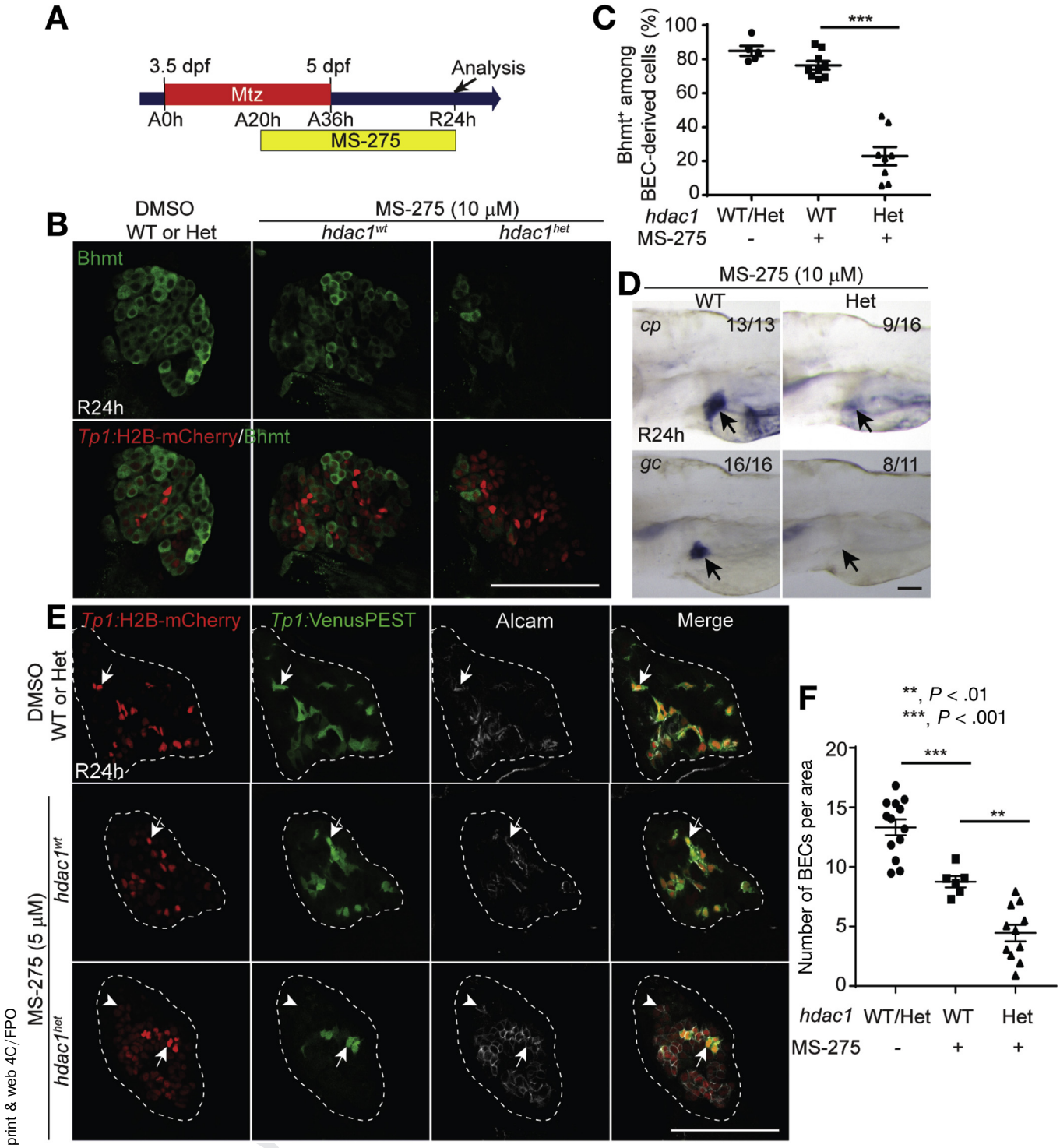

Figure 3. Hdac1 is required for LPC differentiation during regeneration. (*A*) Experimental scheme illustrating the stages of Mtz and MS-275 treatment and analysis (*arrow*). (*B*) Single-optical section images showing Bhmt and *Tp1:*H2B-mCherry expression in regenerating livers at R24h. (*C*) Quantification of the percentage of Bhmt$^+$ hepatocytes among BEC-derived Q26 cells, as shown in *B*. (*D*) WISH images showing *cp* and *gc* expression in regenerating livers at R24h. Arrows point to regenerating livers. (*E*) Confocal projection images showing the expression of Alcam, *Tp1:*VenusPEST, and *Tp1:*H2B-mCherry in regenerating livers at R24h. Arrows point to VenusPEST$^+$/Alcam$^+$ cells (ie, BECs); arrowheads point to VenusPEST$^-$/Alcam$^+$ cells. (*F*) Quantification of BEC number per area, as shown in *E*. Scale bars, 100 μm; error bars show ± standard error of the mean. Het, heterogeneous; M, mol/L; WISH, whole-mount in situ hybridization.

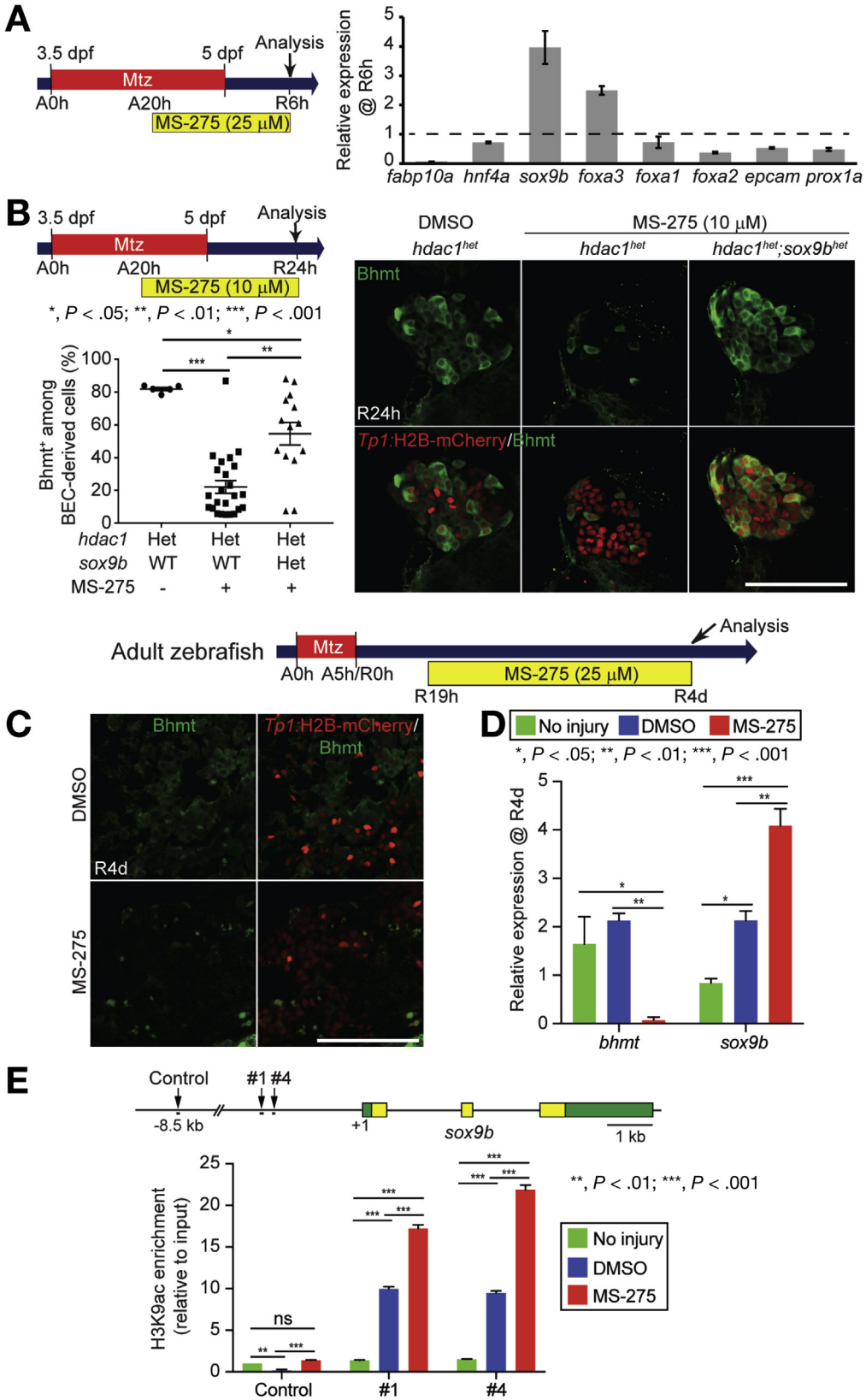

Figure 4. Hdac1 regulates LPC-to-hepatocyte differentiation by repressing *sox9b* expression. (*A*) qPCR data showing the relative expression levels of *fabp10a, hnf4a, sox9b, foxa1/2/3, epcam,* and *prox1a* between DMSO- and MS-275–treated regenerating livers at R6h. (*B*) Single-optical section images showing Bhmt and *Tp1:*H2B-mCherry expression in regenerating livers at R24h. Quantification of the percentage of Bhmt$^+$ hepatocytes among BEC-derived cells is shown. (*C*) Single-optical section images showing Bhmt and *Tp1:*H2B-mCherry expression in regenerating livers of adult zebrafish at R4d. (*D*) qPCR data showing the relative expression levels of *bhmt* and *sox9b* among uninjured control livers, DMSO- and MS-275–treated regenerating livers at R4d. (*E*) ChIP-qPCR data showing the relative enrichment of the selected *sox9b* promoter regions among uninjured control livers, DMSO- and MS-275–treated regenerating livers at R4d, after immunoprecipitation with H3K9ac antibody. Scheme illustrates the *sox9b* genomic locus. Arrows point to the regions amplified by qPCR. Green and yellow boxes denote untranslated and coding regions, respectively. Scale bars, 100 μm; error bars show ± standard error of the mean. M, mol/L; ns, not significant; WT, wild type.

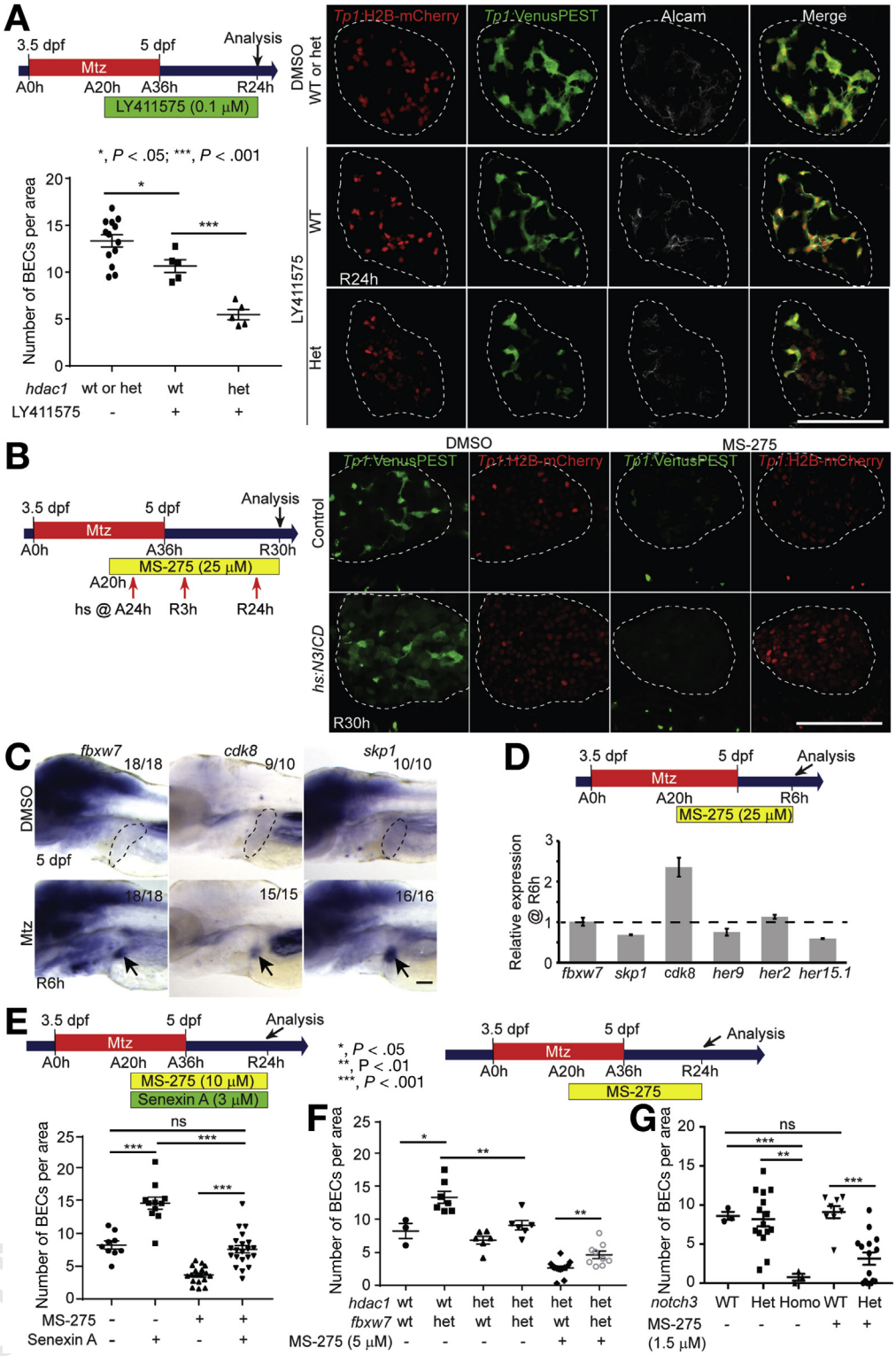

Figure 5. Hdac1 regulates LPC-to-BEC differentiation via Cdk8, Fbxw7 and Notch3. (*A*) Confocal projection images showing the expression of *Tp1:*H2B-mCherry, *Tp1:* VenusPEST, and Alcam in regenerating livers (dashed lines) at R24h. Quantification of VenusPEST$^+$/Alcam$^+$ cell (ie, BEC) number is shown. (*B*) Single-optical section images showing *Tp1:* VenusPEST and *Tp1:*H2B-mCherry expression in regenerating livers (dashed lines) at R30h. *hs:*N3ICD expression was induced by multiple heat shocks at A24h, R3h, and R24h. (*C*) WISH images showing *fbxw7, cdk8,* and *skp1* expression in normal livers (dashed lines) at 5 dpf and regenerating livers (arrows) at R6h. (*D*) qPCR data showing the relative expression levels of *fbxw7, skp1, cdk8, her9, her2,* and *her15.1* between DMSO- and MS-275–treated regenerating livers at R6h. (*E–G*) Quantification of BEC number per area, as shown in Supplementary Figures 5*A* and *B* and 6*A*, respectively. Scale bars, 100 μm; error bars show ± standard error of the mean. Het, heterogeneous; M, mol/L WISH, whole-mount in situ hybridization; wt, wild type.

in MS-275–treated regenerating livers (Figure 2*B–E*) might be caused by reduced Notch activity. To test this hypothesis, we treated *hdac1*$^{+/-}$ larvae with a low dose of the Notch inhibitor LY411575.[34] The treatment of 0.1 μmol/L LY411575 reduced BEC numbers greatly in *hdac1*$^{+/-}$, but moderately in wild-type, regenerating livers (Figure 5*A*), suggesting that *hdac1*$^{+/-}$ regenerating livers exhibited reduced Notch activity compared with the wild type. We aimed to rescue the BEC defect observed in MS-275–treated regenerating livers by enhancing Notch activity with the *Tg(hs:N3ICD)* line that expresses Notch3 intracellular domain upon heat shock.[35] Although the BEC defect was not

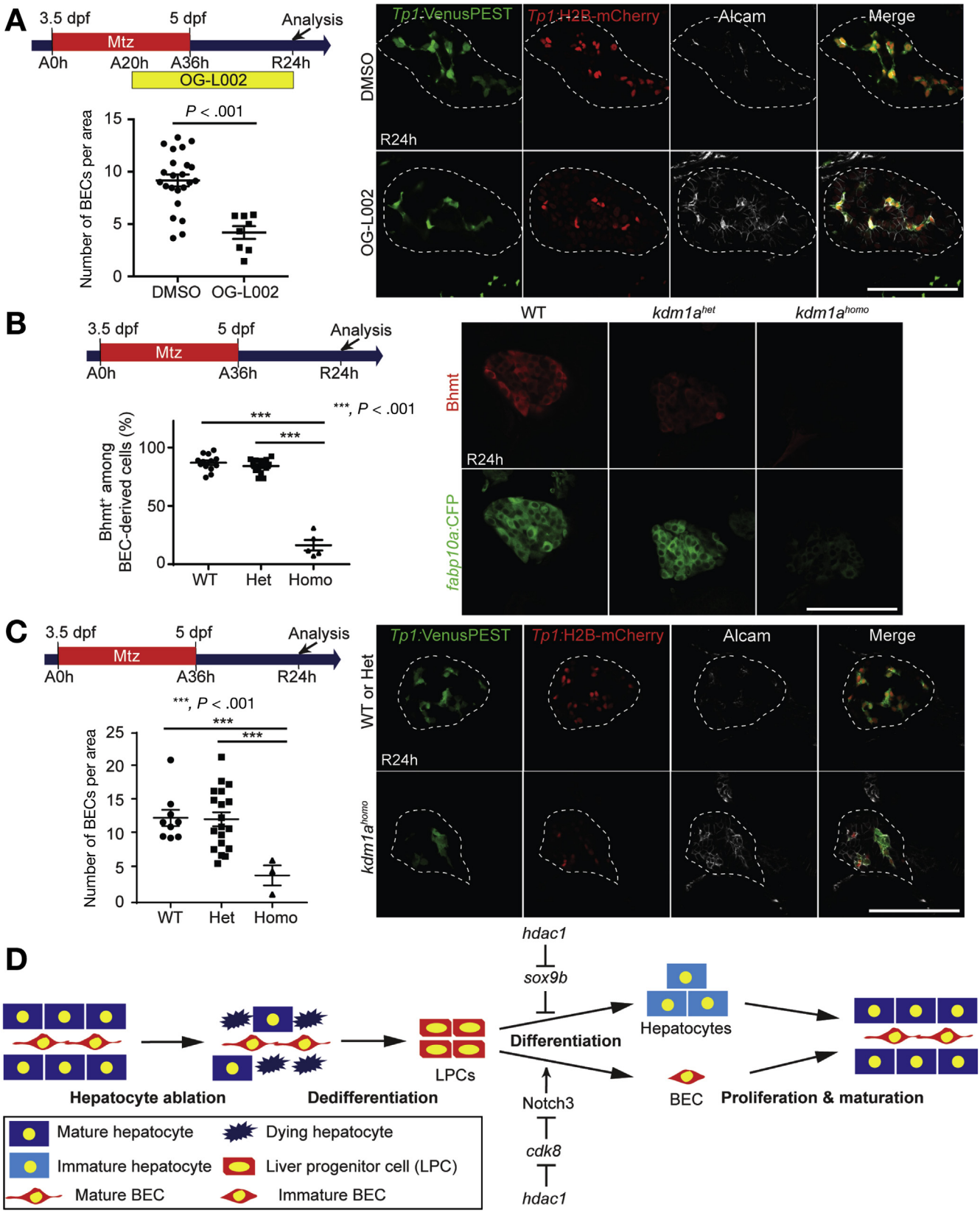

Figure 6. Kdm1a regulates LPC differentiation during regeneration. (*A*, *C*) Confocal projection images showing the expression of Alcam, *Tp1:*VenusPEST, and *Tp1:*H2B-mCherry in regenerating livers (dashed lines) at R24h. Quantification of BEC number per area is shown. (*B*) Single-optical section images showing Bhmt and *Tp1:*H2B-mCherry expression in regenerating livers at R24h. Quantification of the percentage of Bhmt$^+$ hepatocytes among BEC-derived cells is shown; both strong and weak Bhmt expression were considered Bhmt$^+$. (*D*) The process of BEC-driven liver regeneration upon massive hepatocyte ablation in zebrafish larvae, focusing on the role of Hdac1 in LPC differentiation into hepatocytes and BECs. Scale bars,100 μm; error bars show ± standard error of the mean. WT, wild type.

rescued, we observed that ectopic Notch activity induced by *hs:*N3ICD expression disappeared much faster in MS-275–treated regenerating livers than in DMSO-treated regenerating livers, as assessed by *Tp1:*VenusPEST expression. At R30h, 6 hours after the last heat shock, weak but noticeable *Tp1:*VenusPEST expression was observed broadly in DMSO-treated regenerating livers, whereas such expression was barely observed in MS-275–treated regenerating livers (Figure 5*B*), raising a possibility that MS-275 treatment promotes the degradation of Notch intracellular domain (NICD) proteins in regenerating livers. NICD is degraded by the ubiquitin/proteasome pathway: it is first phosphorylated by Cdk8, and then phosphorylated NICD is ubiquitinated by an SCF complex containing an E3 ubiquitin ligase substrate adaptor, Fbxw7.[36] In regenerating livers at R6h, *cdk8*, *fbxw7*, and *skp1*, a core component gene of the SCF complex,[37] were up-regulated (Figure 5*C*), and *cdk8* expression was further increased in MS-275–treated regenerating livers (Figure 5*D*). Intrigued by this up-regulation, we tested whether reducing Cdk8 activity could restore the reduced BEC number phenotype observed in MS-275–treated regenerating livers. Indeed, the treatment of the Cdk8 inhibitor, senexin A,[38] restored the BEC number to normal levels (Figure 5*E* and Supplementary Figure 5*A*). Moreover, reducing Fbxw7 level with *fbxw7* heterozygous mutants restored, albeit in part, the reduced BEC number in MS-275–treated *hdac1*$^{+-}$ mutants (Figure 5*F* and Supplementary 5*B*). BEC numbers in regenerating livers at R24h were increased in both senexin A-treated larvae and *fbxw7*$^{+/-}$ mutants (Figure 5*E* and *F*), further supporting that enhanced Notch activity results in excessive BECs. These increased BEC numbers were also restored to the normal number upon Hdac1 repression (senexin A vs senexin A/MS-275 co-treatment in Figure 5*E*; *fbxw7*$^{+/-}$ vs *fbxw7*$^{+/-}$;*hdac1*$^{+/-}$ in Figure 5*F*). Altogether, these data indicate that Hdac1 regulates LPC-to-BEC differentiation during regeneration by positively controlling Notch activity through the repression of Cdk8/Fbxw7-mediated degradation of NICD.

Notch3 Is Required for LPC-to-BEC Differentiation During Regeneration

We next determined which Notch receptor(s) regulated LPC differentiation during regeneration. Given its biliary-restricted expression,[39] we examined whether *notch3* was implicated in BEC-driven liver regeneration. The *notch3*$^{-/-}$ mutants exhibited the normal differentiation of LPCs into hepatocytes in regenerating livers at R24h, as assessed by Bhmt expression (Supplementary Figure 6*B*). By contrast, *notch3*$^{-/-}$ mutants had few BECs in regenerating livers at R24h (Figure 5*G* and Supplementary Figure 6*A*), indicating Notch3 as the essential Notch receptor for BEC-driven liver regeneration, particularly LPC-to-BEC differentiation. Using *notch3*$^{+/-}$ mutants, which have the normal number of BECs in regenerating livers, we determined whether the treatment of a suboptimal dose of MS-275 could reduce the number of BECs in the regenerating livers of *notch3*$^{+/-}$, but not wild-type, larvae. The treatment of 1.5 μmol/L MS-275 did not affect BEC number in wild-type regenerating livers but significantly reduced its number in *notch3*$^{+/-}$ regenerating livers at R24h (Figure 5*G*). Altogether, these *notch3* mutant data show the essential role of Notch3 in LPC-to-BEC differentiation during regeneration and further support the notion that Hdac1 regulates this differentiation process by positively controlling Notch signaling.

Kdm1a Also Regulates LPC Differentiation Into Either Hepatocytes or BECs During Regeneration

Given that Kdm1a suppression with OG-L002 blocked LPC-to-hepatocyte differentiation (Figure 1*B*) and that Kdm1a and Hdac1 often function in the same repressive complexes,[21] we hypothesized that Kdm1a suppression also blocked LPC-to-BEC differentiation as observed upon Hdac1 suppression. Indeed, OG-L002 treatment greatly reduced BEC number in regenerating livers at R24h (Figure 6*A*). Furthermore, *kdm1a*$^{-/-}$ mutants also exhibited the defects in LPC differentiation: in regenerating livers at R24h, *kdm1a*$^{-/-}$ mutants displayed almost no Bhmt expression (Figure 6*B*) and significantly reduced BEC number compared with their siblings (Figure 6*C*). Altogether, these Kdm1a data suggest that Hdac1 and Kdm1a co-regulate LPC differentiation during regeneration.

Evidence in Mammals That Supports the Role of Hdac1 in LPC-to-Hepatocyte Differentiation

To determine whether the role of Hdac1 in LPC differentiation is conserved in mammals, we examined the effect of MS-275 on LPC-to-hepatocyte differentiation in a new mouse liver injury model, in which a small subset of BEC-derived LPCs contribute to hepatocytes.[40] In this model, hepatocyte-specific deletion of the β-catenin gene, *Ctnnb1*, (knockout [KO]) nearly completely prevents hepatocyte proliferation after choline-deficient, ethionine-supplemented (CDE) diet–induced liver injury, permitting β-catenin$^+$ BECs to give rise to hepatocytes. KO mice were fed a CDE diet for 2 weeks, followed by recovery on a normal chow diet for 7 days; MS-275 or vehicle was intraperitoneally injected daily from R1d during the recovery phase (Figure 7*A*). There was no significant difference between DMSO- and MS-275–injected regenerating mice at R7d in body weight, liver weight, and serum liver injury marker levels (Supplementary Figure 7), suggesting that MS-275 administration did not exacerbate liver damage. Expectedly, MS-275 administration increased the levels of acetylation of histone H3 at lysine 27 and H3K9ac in the liver (Figure 7*E*). In DMSO-injected regenerating livers at R7d, a significant number of CK19$^-$/HNF4A$^+$/β-catenin$^+$ hepatocytes (BEC-derived hepatocytes in the KO mice) were observed, whereas in MS-275–injected regenerating livers, their number was greatly reduced (Figure 7*B*, *arrows*). We found that the proliferation rate of the BEC-derived hepatocytes was comparable between DMSO- and MS-275–injected regenerating livers (Figure 7*C*, arrows), ruling out the possibility that the decrease in their number in

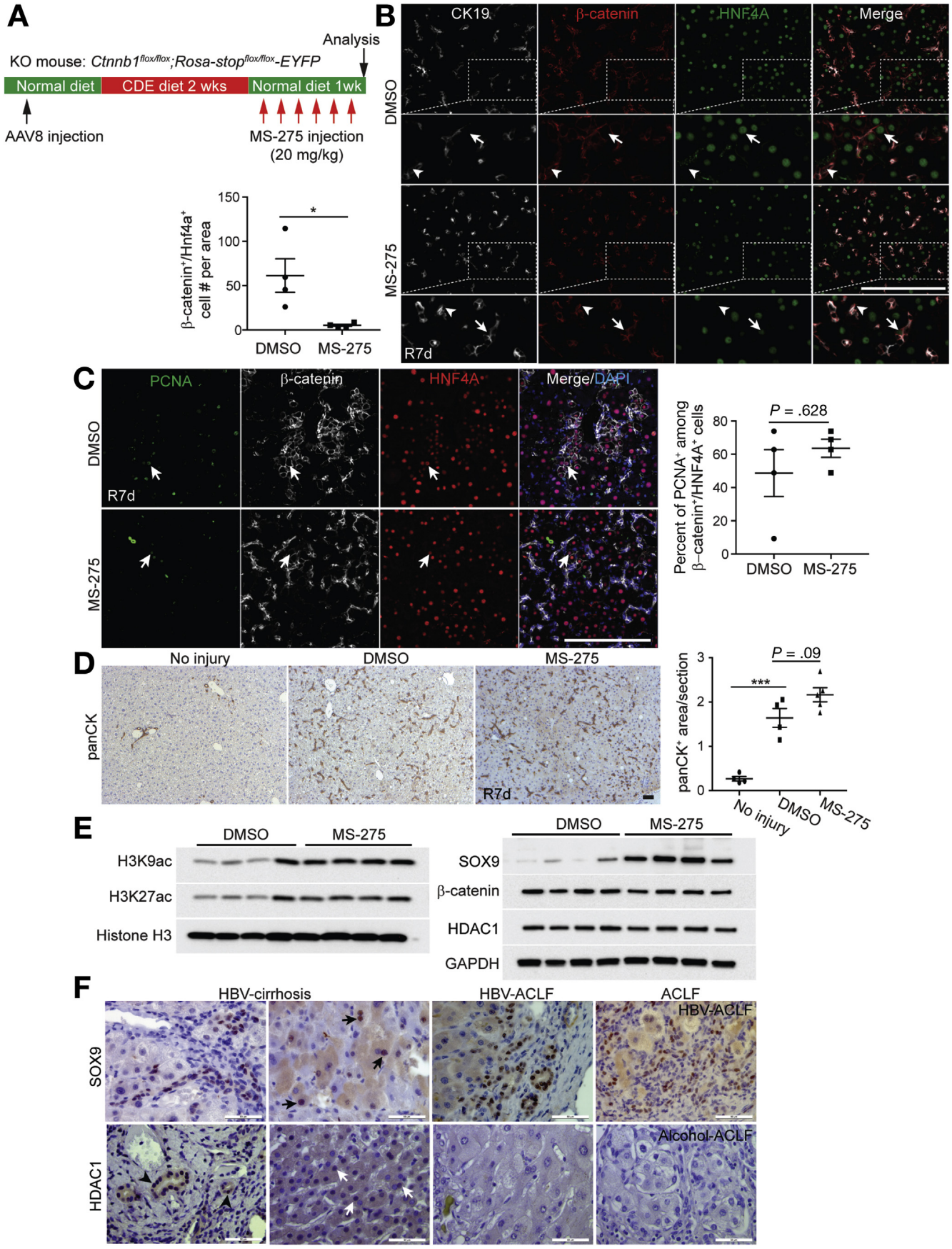

MS-275–injected regenerating livers is due to reduced proliferation. Moreover, although not significant, overall ductular reactions were slightly increased in MS-275–injected regenerating livers (Figure 7*D*). We also found that MS-275 injection increased SOX9 expression in the regenerating livers (Figure 7*E*), as observed in zebrafish. Collectively, these mouse data strongly support the findings from zebrafish that Hdac1 regulates LPC-to-hepatocyte differentiation during regeneration.

Next, we investigated HDAC1 and SOX9 expression in human livers with advanced liver diseases by examining 15 patient liver specimens with 3 types of cirrhosis: compensated, decompensated, and acute-on-chronic liver failure (ACLF). SOX9 expression was detected in BECs and most reactive ducts in all measured specimens (Supplementary Table 6). Although a few hepatocytes inside of hepatocyte buds showed SOX9 expression (Figure 7*F*, *arrows*), most hepatocyte buds did not express SOX9 (Figure 7*F*). Among 15 patients, HDAC1 expression was detected in 7 hepatitis B virus (HBV)–associated cirrhotic patients, either compensated or decompensated; however, it was undetectable in alcohol-associated decompensated cirrhotic and ACLF patients (Figure 7*F* and Supplementary Table 6). HDAC1 was expressed in reactive ducts and hepatocytes (Figure 7*F*, *arrowheads* and *white arrows*, respectively). HBV-associated cirrhotic livers strongly expressed HDAC1 in hepatocyte buds, whereas SOX9 expression in these LPC-derived hepatocytes was undetectable (Figure 7). It is worth noting that the ACLF patients, who received liver transplantation, did not have the detectable, hepatic expression of HDAC1 (Figure 7*F*). Their livers were full of SOX9$^+$ reactive ducts (Figure 7*F*), implying a defect in LPC-to-hepatocyte differentiation. Whether ACLF patients who spontaneously recovered express HDAC1 requires further investigation. In addition, in contrast to HBV-associated cirrhosis, 2 alcohol-associated decompensated cirrhotic patients did not express HDAC1 (Supplementary Table 6). This might explain the previous study showing that LPCs failed to differentiate into hepatocytes in patients with alcoholic hepatitis.[41] Collectively, these human data suggest the conserved role of HDAC1 in LPC-to-hepatocyte differentiation.

Discussion

In this study, we provide novel molecular mechanisms by which Hdac1 regulates differentiation of LPCs into either hepatocytes or BECs during regeneration. These fate decisions have usually been studied using LPCs isolated and established from diseased livers in vitro. Although such in vitro studies have shown the molecular mechanisms underlying LPC differentiation,[13,42] findings from the in vitro studies need to be validated in vivo. However, lack of in vivo models in which LPCs efficiently differentiate into both hepatocytes and BECs during regeneration has prevented such in vivo validation. Recently, liver injury models in which BECs, via LPCs, extensively contribute to hepatocytes have been established in zebrafish[5–7] and mice.[8–10] Particularly in the zebrafish model, liver regeneration occurs through differentiation of LPCs into both hepatocytes and BECs; therefore, this model can be used not only to validate findings from in vitro studies but also to show novel molecular mechanisms underlying LPC differentiation during regeneration. Using the zebrafish model, we show that 1) Hdac1 represses *sox9b* expression, thereby permitting LPC-to-hepatocyte differentiation, and that 2) Hdac1 represses *cdk8* expression, thereby enhancing Notch signaling, which induces LPC-to-BEC differentiation (Figure 6*D*). These findings not only confirm the known role of Notch signaling in LPC-to-BEC differentiation,[13,14,42] but they also reveal 3 crucial genes (*cdk8*, *fbxw7*, and *notch3*) that regulate Notch signaling during liver regeneration, which is further supported by an in vitro study showing that *Fbxw7* deficiency skews the differentiation of mouse LPCs toward BECs.[43] Complementary to these findings from zebrafish, we also provide evidence of the role of Hdac1 in LPC-to-hepatocyte differentiation in mice and humans.

Despite its wide use in the liver field as a BEC/LPC marker and a lineage tracing tool,[44] the role of Sox9 in liver injury settings remains largely unknown. In this study, we show the repressive role of Sox9b in LPC-to-hepatocyte differentiation. This finding is supported by an in vitro study showing the negative role of SOX9 in the differentiation of human LPCs into hepatocytes.[45] This role of Sox9b is rather consistent with the role of mammalian SOX9 in the maintenance of stemness and the inhibition of differentiation in liver cancer[30] and mammary[31] stem cells and kidney progenitor cells.[46] SOX9 is restrictively expressed in BECs in the normal liver; however, its expression is often induced in hepatocytes in various rodent liver injury models[47] and in human liver diseases.[45] Based on our finding about the role of Sox9b in LPCs, we speculate that SOX9 expression in hepatocytes may make them lose their cellular identity,

Figure 7. Evidence in mammals that supports the role of Hdac1 in LPC-to-hepatocyte differentiation. (*A*) Experimental scheme illustrating the period of a CDE diet, AAV8 and MS-275 injection stages, and analysis stage. (*B*) Section confocal images showing CK19, HNF4A, and β-catenin expression in regenerating mouse livers at R7d. Arrows point to BEC-derived hepatocytes (CK19$^-$/HNF4A$^+$/β-catenin$^+$); arrowheads to BECs (CK19$^+$/HNF4A$^-$/β-catenin$^+$). (*C*) Section confocal images showing PCNA, HNF4A and β-catenin expression with 4′,6-diamidino-2-phenylindole (DAPI) staining in regenerating livers at R7d. Arrows point to PCNA$^+$/HNF4A$^+$/β-catenin$^+$ hepatocytes. Quantification of the percentage of PCNA$^+$ among BEC-derived hepatocytes is shown. (*D*) Section images showing anti-pan-cytokeratin (panCK) immunostaining. Quantification of panCK$^+$ area is shown. (*E*) Western blot images of whole-liver lysate from DMSO- or MS-275–injected regenerating livers at R7d. (*F*) Human liver section images showing SOX9 and HDAC1 expression. Arrows point to SOX9$^+$ hepatocytes, arrowheads to HDAC1$^+$ reactive ducts, and white arrows to HDAC1$^+$ hepatocytes. *Scale bars*, 100 μm (*B–D*) and 50 μm (*F*); error bars show ± standard error of the mean. DAPI, 4′,6-diamidino-2-phenylindole; GAPDH, glyceraldehyde-3-phosphate dehydrogenase (phosphorylating).

thereby promoting their dedifferentiation into oval cells (ie, LPCs) and simultaneously preventing their differentiation into hepatocytes. It will be interesting to examine in mice if hepatocyte- or BEC-specific deletion of *Sox9* results in any defect in LPC-driven liver regeneration.

It was previously suggested that in hepatocyte injury settings, such as the CDE model, Wnt/β-catenin signaling activated by macrophage-derived Wnt3a represses Notch activity in LPCs by inducing *Numb* expression, thereby promoting differentiation of LPCs into hepatocytes.[13] It was also suggested that in biliary injury settings, such as the 3,5-diethoxycarbonyl-1,4-dihydrocollidine model, Notch signaling activated by myofibroblast-derived Jagged1 promotes LPC differentiation into BECs.[13] However, more recent in vivo studies showed that either the activation of Wnt/β-catenin signaling or the inhibition of Notch signaling in BECs/LPCs was not sufficient to differentiate 3,5-diethoxycarbonyl-1,4-dihydrocollidine–induced LPCs into hepatocytes,[48] indicating that additional factors regulate this differentiation process. In our study, reduction of Sox9b expression rescued a defect in LPC-to-hepatocyte differentiation observed in Hdac1-repressed regenerating livers, suggesting Sox9 as the additional factor that regulates LPC-to-hepatocyte differentiation. As a key component of multiple transcriptional repressor complexes,[49] Hdac1 represses the expression of numerous genes by removing acetylation marks on the lysine residues of histones. Therefore, it is surprising that reducing the expression level or the activity of a single gene is sufficient to rescue a defect in LPC differentiation observed in Hdac1-repressed larvae: *sox9b* for LPC-to-hepatocyte differentiation and *cdk8* or *fbxw7* for LPC-to-BEC differentiation. Likewise, reducing the expression level of *Bmp4* with *Bmp4*$^{+/-}$ mutants rescued a defect in proximal airway development observed in foregut endoderm-specific *Hdac1/2* double-KO mice.[25]

During development, Sox9 is not required for differentiation of hepatoblasts into BECs in mice[50] or zebrafish,[23] whereas Sox9 appears to regulate LPC-to-BEC differentiation during regeneration, as suggested by the reduced BEC number in *sox9b*$^{+/-}$ regenerating livers (Supplementary Figure 4*B*). It was recently reported that both *Sox4* and *Sox9* deletion is required for blocking hepatoblast-to-BEC differentiation,[51] indicating that *Sox4* compensates for the absence of *Sox9* in the developing liver. However, during BEC-driven liver regeneration, other genes, such as *Sox4*, do not compensate for the absence of *Sox9*. Likewise, Notch3 is not required for hepatoblast-to-BEC differentiation during development because of the compensation by Notch2.[52] However, the absence of BECs in regenerating livers of *notch3*$^{-/-}$ mutants (Supplementary Figure 6*A*) indicates the failed compensation by other Notch receptors during BEC-driven liver regeneration. It is tempting to speculate that developmental processes have more compensatory mechanisms than regeneration processes, because every animal goes through developmental processes for its survival, but only a subset of animals go through regeneration processes for their survival.

In summary, we provide the molecular mechanisms underlying LPC differentiation into either hepatocytes or BECs. Given the potential of promoting innate liver regeneration as therapeutics for advanced human liver diseases, a better understanding of the molecular mechanisms underlying LPC-driven liver regeneration is crucial for developing such a therapy. Not only does our finding that Hdac1 regulates LPC differentiation via Sox9b and Cdk8-Fbxw7-Notch3 show novel molecular mechanisms underlying LPC differentiation, but it also suggests a means to repress Sox9 expression or function as a potential therapy to promote liver regeneration in patients with advanced liver diseases.

Supplementary Material

Q22

Note: To access the supplementary material accompanying this article, visit the online version of Gastroenterology at www.gastrojournal.org, and at https://doi.org/10.1053/j.gastro.2018.09.039.

References

1. Miyajima A, Tanaka M, Itoh T. Stem/progenitor cells in liver development, homeostasis, regeneration, and reprogramming. Cell Stem Cell 2014;14:561–574.
2. Duncan AW, Dorrell C, Grompe M. Stem cells and liver regeneration. Gastroenterology 2009;137:466–481.
3. Lowes KN, Brennan BA, Yeoh GC, et al. Oval cell numbers in human chronic liver diseases are directly related to disease severity. Am J Pathol 1999;154:537–541.
4. Lukacs-Kornek V, Lammert F. The progenitor cell dilemma: cellular and functional heterogeneity in assistance or escalation of liver injury. J Hepatol 2017;66:619–630.
5. Choi TY, Ninov N, Stainier DY, et al. Extensive conversion of hepatic biliary epithelial cells to hepatocytes after near total loss of hepatocytes in zebrafish. Gastroenterology 2014;146:776–788.
6. Huang MB, Chang A, Choi M, et al. Antagonistic interaction between Wnt and Notch activity modulates the regenerative capacity of a zebrafish fibrotic liver model. Hepatology 2014;60:1753–1766.
7. He J, Lu H, Zou Q, et al. Regeneration of liver after extreme hepatocyte loss occurs mainly via biliary transdifferentiation in zebrafish. Gastroenterology 2014;146:789–800.
8. **Lu W-Y, Bird TG**, Boulter L, et al. Hepatic progenitor cells of biliary origin with liver repopulation capacity. Nat Cell Biol 2015;17:971–983.
9. **Raven A, Lu WY**, Man TY, et al. Cholangiocytes act as facultative liver stem cells during impaired hepatocyte regeneration. Nature 2017;547:350–354.
10. **Deng X, Zhang X, Li W**, et al. Chronic liver injury induces conversion of biliary epithelial cells into hepatocytes. Cell Stem Cell 2018;23:114–122.
11. Stueck AE, Wanless IR. Hepatocyte buds derived from progenitor cells repopulate regions of parenchymal

extinction in human cirrhosis. Hepatology 2015;61:1696–1707.
12. **Ko S, Choi TY**, Russell JO, et al. Bromodomain and extraterminal (BET) proteins regulate biliary-driven liver regeneration. J Hepatol 2016;64:316–325.
13. Boulter L, Govaere O, Bird TG, et al. Macrophage-derived Wnt opposes Notch signaling to specify hepatic progenitor cell fate in chronic liver disease. Nat Med 2012;18:572–579.
14. Spee B, Carpino G, Schotanus BA, et al. Characterisation of the liver progenitor cell niche in liver diseases: potential involvement of Wnt and Notch signalling. Gut 2010;59:247–257.
15. Onder TT, Kara N, Cherry A, et al. Chromatin-modifying enzymes as modulators of reprogramming. Nature 2012;483:598–602.
16. Zhu Z, Chen J, Xiong JW, et al. Haploinsufficiency of Def activates p53-dependent TGFbeta signalling and causes scar formation after partial hepatectomy. PLoS One 2014;9:e96576.
17. Hu ED, Dul E, Sung CM, et al. Identification of novel isoform-selective inhibitors within class I histone deacetylases. J Pharmacol Exp Ther 2003;307:720–728.
18. Bradner JE, West N, Grachan ML, et al. Chemical phylogenetics of histone deacetylases. Nat Chem Biol 2010;6:238–243.
19. Hoshikawa Y, Kwon HJ, Yoshida M, et al. Trichostatin A induces morphological changes and gelsolin expression by inhibiting histone deacetylase in human carcinoma cell lines. Exp Cell Res 1994;214:189–197.
20. Liang Y, Quenelle D, Vogel JL, et al. A novel selective LSD1/KDM1A inhibitor epigenetically blocks herpes simplex virus lytic replication and reactivation from latency. MBio 2013;4. e00558-12.
21. Lee MG, Wynder C, Cooch N, et al. An essential role for CoREST in nucleosomal histone 3 lysine 4 demethylation. Nature 2005;437:432–435.
22. Ninov N, Borius M, Stainier DYR. Different levels of Notch signaling regulate quiescence, renewal and differentiation in pancreatic endocrine progenitors. Development 2012;139:1557–1567.
23. **Delous M, Yin C**, Shin D, et al. Sox9b is a key regulator of pancreaticobiliary ductal system development. PLoS Genet 2012;8:e1002754.
24. Xia J, Zhou YJ, Ji HJ, et al. Loss of histone deacetylases 1 and 2 in hepatocytes impairs murine liver regeneration through Ki67 depletion. Hepatology 2013;58:2089–2098.
25. Wang Y, Tian Y, Morley MP, et al. Development and regeneration of Sox2+ endoderm progenitors are regulated by a Hdac1/2-Bmp4/Rb1 regulatory pathway. Dev Cell 2013;24:345–358.
26. Noel ES, Casal-Sueiro A, Busch-Nentwich E, et al. Organ-specific requirements for Hdac1 in liver and pancreas formation. Developmental Biology 2008;322:237–250.
27. Hanley KP, Oakley F, Sugden S, et al. Ectopic SOX9 mediates extracellular matrix deposition characteristic of organ fibrosis. J Biol Chem 2008;283:14063–14071.
28. Liu S, Cheng H, Kwan W, et al. Histone deacetylase inhibitors induce growth arrest, apoptosis, and differentiation in clear cell sarcoma models. Mol Cancer Ther 2008;7:1751–1761.
29. Lin SC, Chou YT, Jiang SS, et al. Epigenetic switch between SOX2 and SOX9 regulates cancer cell plasticity. Cancer Res 2016;76:7036–7048.
30. **Liu C, Liu L**, Chen X, et al. Sox9 regulates self-renewal and tumorigenicity by promoting symmetrical cell division of cancer stem cells in hepatocellular carcinoma. Hepatology 2016;64:117–129.
31. Guo W, Keckesova Z, Donaher JL, et al. Slug and Sox9 cooperatively determine the mammary stem cell state. Cell 2012;148:1015–1028.
32. Zong Y, Panikkar A, Xu J, et al. Notch signaling controls liver development by regulating biliary differentiation. Development 2009;136:1727–1739.
33. Burns FR, Lanham KA, Xiong KM, et al. Analysis of the zebrafish sox9b promoter: Identification of elements that recapitulate organ-specific expression of sox9b. Gene 2016;578:281–289.
34. Fauq AH, Simpson K, Maharvi GM, et al. A multigram chemical synthesis of the gamma-secretase inhibitor LY411575 and its diastereoisomers. Bioorg Med Chem Lett 2007;17:6392–6395.
35. Wang Y, Pan L, Moens CB, et al. Notch3 establishes brain vascular integrity by regulating pericyte number. Development 2014;141:307–317.
36. Fryer CJ, White JB, Jones KA. Mastermind recruits CycC: CDK8 to phosphorylate the notch ICD and coordinate activation with turnover. Molecular Cell 2004;16:509–520.
37. Lee EK, Diehl JA. SCFs in the new millennium. Oncogene 2014;33:2011–2018.
38. **Porter DC, Farmaki E**, Altilia S, et al. Cyclin-dependent kinase 8 mediates chemotherapy-induced tumor-promoting paracrine activities. Proc Natl Acad Sci U S A 2012;109:13799–13804.
39. So J, Khaliq M, Evason K, et al. Wnt/beta-catenin signaling controls intrahepatic biliary network formation in zebrafish by regulating notch activity. Hepatology 2018;67:2352–2366.
40. Russell JO, Lu WY, Okabe H, et al. Hepatocyte-specific beta-catenin deletion during severe liver injury provokes cholangiocytes to differentiate into hepatocytes. Hepatology. In press. Q23
41. Sancho-Bru P, Altamirano J, Rodrigo-Torres D, et al. Liver progenitor cell markers correlate with liver damage and predict short-term mortality in patients with alcoholic hepatitis. Hepatology 2012;55:1931–1941.
42. Kitade M, Factor VM, Andersen JB, et al. Specific fate decisions in adult hepatic progenitor cells driven by MET and EGFR signaling. Genes Dev 2013;27:1706–1717.
43. Onoyama I, Suzuki A, Matsumoto A, et al. Fbxw7 regulates lipid metabolism and cell fate decisions in the mouse liver. J Clin Invest 2011;121:342–354.
44. Tarlow BD, Finegold MJ, Grompe M. Clonal tracing of Sox9+ liver progenitors in mouse oval cell injury. Hepatology 2014;60:278–289.
45. **Paganelli M, Nyabi O**, Sid B, et al. Downregulation of Sox9 expression associates with hepatogenic differentiation of

human liver mesenchymal stem/progenitor cells. Stem Cells Dev 2014;23:1377–1391.

46. Kang HM, Huang S, Reidy K, et al. Sox9-positive progenitor cells play a key role in renal tubule epithelial regeneration in mice. Cell Rep 2016;14:861–871.
47. **Yanger K, Zong Y**, Maggs LR, et al. Robust cellular reprogramming occurs spontaneously during liver regeneration. Genes Dev 2013;27:719–724.
48. **Jors S, Jeliazkova P**, Ringelhan M, et al. Lineage fate of ductular reactions in liver injury and carcinogenesis. J Clin Invest 2015;125:2445–2457.
49. Kelly RD, Cowley SM. The physiological roles of histone deacetylase (HDAC) 1 and 2: complex co-stars with multiple leading parts. Biochem Soc Trans 2013; 41:741–749.
50. Antoniou A, Raynaud P, Cordi S, et al. Intrahepatic bile ducts develop according to a new mode of tubulogenesis regulated by the transcription factor SOX9. Gastroenterology 2009;136:2325–2333.
51. Poncy A, Antoniou A, Cordi S, et al. Transcription factors SOX4 and SOX9 cooperatively control development of bile ducts. Dev Biol 2015;404:136–148.
52. Lorent K, Yeo SY, Oda T, et al. Inhibition of Jagged-mediated Notch signaling disrupts zebrafish biliary development and generates multi-organ defects compatible with an Alagille syndrome phenocopy. Development 2004; 131:5753–5766.

Author names in bold designate shared co-first authorship.

Received March 2, 2017. Accepted September 18, 2018.

Reprint requests
Address requests for reprints to: Donghun Shin, PhD, 3501 5th Avenue, #5063, Pittsburgh, Pennsylvania 15260. e-mail: donghuns@pitt.edu; fax: (412) 383-2211. Sungjin Ko, PhD, DVM, 200 Lothrop Street, Room S451, Pittsburgh, Pennsylvania 15261. e-mail: sungjin@pitt.edu; fax: (412) 648-1916. Q6 Q7 Q8

Acknowledgments
We thank Paul Henion and Christine Beattie for *hdac1* and Bruce Appel for *fbxw7* and *notch3* mutant lines; Neil Hukriede and Michael Tsang for discussions; and Mehwish Khaliq, Fangqiang Wei, and Andy Duncan for critical reading of the manuscript.

Author contributions: study concept and design: Sungjin Ko and Donghun Shin; data analysis: Sungjin Ko, Jacquelyn O. Russell, Jianmin Tian, Rilu Feng, and Xiaodong Yuan; interpretation of data: Sungjin Ko, Jacquelyn O. Russell, Hong-Lei Weng, Joseph Locker, Satdarshan P. Monga, and Donghun Shin; writing the manuscript: Sungjin Ko and Donghun Shin; material support: Ce Gao, Makoto Kobayashi, Chen Shao, and Huiguo Ding; study supervision: Satdarshan P. Monga and Donghun Shin. Q21

Conflicts of interest
The authors disclose no conflicts. Q9

Funding
The work was supported by National Institutes of Health grants to Donghun Sin (DK101426), Satdarshan P. Monga (DK62277, DK100287, CA204586), Joseph Locker (CA104292), and Jacquelyn O. Russell (T32EB0010216, 1F31DK115017). Satdarshan P. Monga is an Endowed Chair for Experimental Pathology. This work was also supported by the Chinese-German Cooperation Group project (grant number GZ1263) to Huiguo Ding and by the Chinese Nature Science Foundation (grant number 81672725) and the State Key Project Specialized on Infectious Diseases (2017ZX10203202-004) to Huiguo Ding. Q10 Q40

Supplementary Methods

Zebrafish Strains

Embryos and adult fish were raised and maintained under standard laboratory conditions.[1] We used *hdac1*^{b382}, *sox9b*^{fh313}, *fbxw7*^{vu56}, *notch3*^{fh332}, and *kdm1a*^{it627} mutant lines and the following transgenic lines: *Tg(fabp10a:rasGFP)*^{s942}, *Tg(Tp1:VenusPEST)*^{s940}, *Tg(Tp1:H2B-mCherry)*^{s939}, *Tg(fabp10a:CFP-NTR)*^{s931}, and *Tg(hs:N3ICD)*^{co17}. Their full names and references are listed in Supplementary Table 1.

Genotyping of hdac1, sox9b, fbxw7, notch3, and kdm1a Mutants

For *sox9b* genotyping, genomic DNA was amplified with either wild-type allele– (5′-AGACCAGTCGTAGCCCTT-3′) or mutant allele–specific (5′-AGACCAGTCGTAGCCCTA-3′) reverse primer and a common forward primer (5′-TGAGTGTGTCCGGAGCTCCGA-3′). For *notch3* genotyping, genomic DNA was amplified with either wild-type allele– (5′-CATGATCCCTACTGCTAT-3′) or mutant allele–specific (5′-CATGATCCCTACTGCTAG-3′) forward primer and a common reverse primer (5′-CAGTTCTTACCCACCCATCC-3′). For *hdac1* genotyping, genomic DNA was amplified with a forward (5′-CGTAGGGGAGGATTGTCCTGTC-3′) and a reverse (5′-TGAGCAGCTCCAGAATGGCCAG-3′) primer pair; its 294-base pair (bp) PCR products were digested with *EcoRI*, which cut the mutant but not wild-type allele. For *fbxw7* genotyping, genomic DNA was amplified with a forward (5′-TGTGTCAATGTGTTTCGGTTGAGA-3′) and a reverse (5′-CGAAGGGATTTCTCTCACCA-3′) primer pair; its 656-bp PCR products were digested with *BamHI*, which cut the wild-type, but not mutant, allele. *kdm1a* genotyping was performed as previously described.[2]

Chemical Screening

To identify epigenetic regulators that regulate BEC-driven liver regeneration, we screened small molecules from an epigenetic compound library (Cayman Chemical). We also tested additional compounds that inhibit epigenetic regulators but are not present in the library. The working concentration of each compound (total of 41 compounds) was determined by treating larvae in a 96-well plate (3 larvae/well) with various concentrations; the maximum tolerated concentration was used for the screening. The names and working concentrations of the screened compounds are listed in Supplementary Table 2. Hepatocyte ablation was performed by treating *Tg(fabp10a:CFP-NTR);Tg(fabp10a:rasGFP);Tg(Tp1:H2B-mCherry)* larvae with 10 mmol/L Mtz in egg water supplemented with 0.2% DMSO and 0.2 mmol/L 1-phenyl-2-thiourea from 3.5 to 5 dpf for 36 hours. The larvae in a 12-well plate (15 larvae/well) were treated with the selected compounds from A20h to R24h and harvested at R24h for subsequent whole-mount immunostaining with anti-Bhmt. The expression levels of *fabp10a:*rasGFP, *Tp1:*H2B-mCherry, and Bhmt in regenerating livers were shown by a Zeiss LSM700 confocal microscope.

MS-275, Senexin A, OG-L002, and LY411575 Treatment

For MS-275 (Selleckchem) treatment, depending on mutant backgrounds and phenotypes of interest, 1.5, 5, 10, or 25 μmol/L was used for the final concentration. For senexin A (Tocris), LY411575 (Cayman Chemical), and OG-L002 (Selleckchem) treatments, 3, 0.1, and 100 μmol/L were used, respectively.

Whole-Mount In Situ Hybridization and Immunostaining

Whole-mount in situ hybridization was performed as previously described.[3] cDNA from 24-hours-postfertilization embryos or 5-dpf livers was used as a template for PCR to amplify genes of interest; PCR products were used to make in situ probes. The primers used for the probe synthesis are listed in Supplementary Table 3. Whole-mount immunostaining was performed as previously described[4] with the following antibodies: goat anti-Hnf4a (1:50; Santa Cruz Biotechnology), mouse anti-Bhmt (1:400; gift from Jinrong Peng at Zhejiang University), mouse anti-Alcam (Zn5, 1:10; ZIRC), rat anti-mCherry (1:400; Allele Biotechnology), rabbit anti-Hdac1 (1:200; GeneTex), and Alexa Fluor 488-, 568-, and 647-conjugated secondary antibodies (1:500; Life Technologies). Q29

EdU and Terminal Deoxynucleotidyl Transferase–Mediated Deoxyuridine Triphosphate Nick-End Labeling Q30

EdU labeling was performed according to the protocol outlined in the Click-iT EdU Alexa Fluor 647 Imaging Kit (Life Technologies). Larvae were treated with egg water containing 10 mmol/L EdU and 1% DMSO for 5 hours. After the 5-hour EdU treatment, the larvae were harvested for subsequent analysis. Terminal deoxynucleotidyl transferase–mediated deoxyuridine triphosphate nick-end labeling (TUNEL) was performed as described in the protocol of the In Situ Cell Death Detection Kit, TMR red (Roche).

Image Acquisition, Processing, and Statistical Analysis

Zeiss LSM700 confocal and Leica M205 FA epifluorescence microscopes were used to obtain image data. Confocal stacks were analyzed using the Zen 2009 software. All figures, labels, arrows, scale bars, and outlines were assembled or drawn using the Adobe Illustrator software. For analyses concerning only 2 groups, a 2-tailed Student *t* test was performed, with $P < .05$ considered significant. For analyses concerning more than 2 groups, a 1-way analysis of variance test was performed, with $P < .05$ considered significant. Quantitative data were shown as mean ± standard error of the mean.

Heat-Shock Condition

Tg(hs:N3ICD) larvae were heat-shocked by transferring them into egg water prewarmed to 37°C and kept at this temperature for 20 minutes, as previously described.[5]

qPCR

Total RNA was extracted from 100 dissected livers using the RNeasy Mini Kit (Qiagen); cDNA was synthesized from the RNA using the SuperScript III First-Strand Synthesis SuperMix (Life Technologies) according to the kit protocols. qPCR was performed as previously described,[6] using the Bio-Rad iQ5 qPCR machine with the iQ SYBR Green Supermix (Bio-Rad). *eef1a1l1* was used for normalization, as previously described.[7] At least 3 independent experiments were performed. The primers used for qPCR are listed in Supplementary Table 4.

Quantification of BEC Number Per Area

A confocal projection image consisting of 10 optical-section images, with 1-μm intervals, was used to manually count BECs; the total BEC number was divided by the entire liver area calculated by ImageJ software (National Institutes of Health).

Adult Zebrafish Studies

Four-month-old *Tg(fabp10a:CFP-NTR)* adult fish were treated with 5 mmol/L Mtz in system water supplemented with 0.5% DMSO for 5 hours. At 19 hours after Mtz washout (R19h), the fish were treated with 25 μmol/L MS-275 or DMSO in system water until they were killed for analysis. Compound solution was replaced with fresh solution every other day.

ChIP-qPCR Assay

Freshly harvested and pooled livers (DMSO- and MS-275–treated livers at R4d, n = 30 per group) were finely minced on ice and added to phosphate-buffered saline (PBS) containing 1% formaldehyde, 0.1 mol/L phenylmethylsulfonyl fluoride, 0.5 mol/L EDTA, and Halt inhibitor cocktail (Thermo Fisher Scientific). Tissue was cross-linked for 15 minutes on a rotator at room temperature, followed by quenching with 0.125 mol/L glycine and rinsing with cold PBS. Tissue was then homogenized in cold PBS plus additives with a Wheaton overhead homogenizer. After pelleting, cells from tissue were lysed in 5-mmol/L piperazine-*N,N′*-bis(2-ethanesulfonic acid) (pH 8.0), 85 mmol/L KCl, and 0.5% NP40 using a Dounce homogenizer and incubated on ice for 15 minutes to release nuclei. Nuclei were resuspended in 50 mmol/L Tris (pH 8.1), 10 mmol/L EDTA, 1% sodium dodecyl sulfate, and inhibitors at 5 times the cell volume and incubated on ice for 20 minutes, then sonicated with a Bioruptor (Diagenode) at 15-minute intervals until chromatin fragments were 200–500 bp in length. At this point, 25 μL of the chromatin fragments was removed and saved as an input. Chromatin aliquots were diluted in IP dilution buffer and precleared with Protein G-Sepharose beads (GE Healthcare) for 3 hours at 4°C. Supernatants were incubated overnight at 4°C with 10 μg of H3K9ac (Abcam, ab4729). Antibody-chromatin complexes were recovered by incubation with Protein G-Sepharose for 3 hours at 4°C and then centrifuged. Additional IP buffer was added to each sample, and then samples were loaded onto a ChIP filtration column (CHIP-IT High Sensitivity Kit, Active Motif) and gravity filtered, followed by washing and elution by centrifugation. Samples were de-crosslinked by incubation with proteinase K at 55°C for 30 minutes, followed by 80°C for 2 hours, and then were purified with the MiniElute kit (Qiagen). The resulting DNA fragments and input controls were subjected to qPCR using primer sets listed in Supplementary Table 5.

Initially, 14 genomic loci within the 3-kb region upstream of *sox9b* TSS (−3 kb to +1) were randomly selected to make 14 sets of primer pairs. Among the 14 sets, sets 1 and 4 exhibited the lowest cycle threshold value by qPCR with input DNA. Thus, these 2 sets were further selected for H3K9ac enrichment analysis. Results in Figure 4*E* represent pooled samples from livers (n = 30) per treatment group assayed in triplicate. ChIP-qPCR data were normalized to percent input for each sample to determine fold change.

Mouse Studies

Ctnnb1$^{flox/flox}$;*Rosa-stop*$^{flox/flox}$*-EYFP* reporter mice were generated through breeding *Ctnnb1*$^{flox/flox}$ mice with *Rosa-stop*$^{flox/flox}$*-EYFP* mice (Jackson Laboratories). To delete β-catenin in hepatocytes, 23–25-day-old *Ctnnb1*$^{flox/flox}$;*Rosa-stop*$^{flox/flox}$*-EYFP* mice were injected intraperitoneally with 1×10^{12} genome copies of AAV8-TBG-Cre (Penn Vector Core), followed by a 12-day washout period. For the liver injury time point, 5-week-old AAV8-TBG-Cre–injected mice were given a choline-deficient diet (Envigo Teklad Diets) supplemented with 0.15% ethionine drinking water (Acros Organics, #146170100) for 2 weeks. For recovery time points, animals were switched back to normal chow diet, and 20 mg/kg MS-275 or 25% DMSO in PBS (vehicle) was intraperitoneally injected daily until they were killed for analysis. The doses, route, and timing of administration were based on a previous study[8] and our pilot test showing that increases in histone acetylation occurred 12 hours after the MS-275 injection. Liver tissue and serum were harvested and stored at −80°C until further analyzed. Serum biochemistry analysis was performed by automated methods at the University of Pittsburgh Medical Center clinical chemistry laboratory. All studies were performed according to the guidelines of the National Institutes of Health and the University of Pittsburgh Institutional Animal Use and Care Committee.

Immunofluorescence With Mouse and Adult Zebrafish Liver Tissue

Tissue samples were drop-fixed in 10% buffered formalin overnight, cryopreserved in 30% sucrose in PBS overnight, frozen in OCT compound (Sakura, #4583) and stored at −80°C or, alternatively, were paraffin embedded after formalin fixation. Cryopreserved samples were cut into 5-μm sections, allowed to air dry, and then washed in PBS. Antigen retrieval was performed through pressure cooking for 20 minutes with Dako Target Retrieval Solution (Dako, S1699). After cooling, slides were washed with PBS and permeabilized with 0.1% Triton X-100 in PBS for 20 minutes at room temperature. Samples were washed 3 times with PBS and then blocked with 5% donkey serum in 0.1%

Tween 20 in PBS (antibody diluent) for 30 minutes at room temperature. Antibodies were diluted as follows: β-catenin (Abcam, ab32572; 1:50), Hnf4A (Santa Cruz Biotechnology, sc-6556; 1:50), CK19 (DSHB, TROMA-III-s; 29 μg/mL), PCNA (Santa Cruz Biotechnology, sc-56; 1:1000) in antibody diluent and incubated at 4°C overnight. Samples were washed 3 times in PBS and incubated with the proper fluorescent secondary antibody (AlexaFluor 488/555/647, Invitrogen) diluted 1:500 in antibody diluent for 2 hours at room temperature. Samples were washed 3 times with PBS and incubated with DAPI (Sigma, B2883) for 30 seconds. Samples were washed 3 times with PBS and mounted with ProLong Gold antifade reagent (Invitrogen, P10144). Images were taken on a Nikon Eclipse Ti epifluorescence microscope or a Zeiss LSM700 confocal microscope.

Immunohistochemistry With Mouse Liver Tissue

Tissue samples were drop fixed in 10% buffered formalin for 48 hours before paraffin embedding. Samples were cut into 4-μm sections, deparaffinized, and washed with PBS. For antigen retrieval, samples were microwaved for 12 minutes in pH 6 sodium citrate buffer (PanCK) or were pressure cooked for 20 minutes in pH 6 sodium citrate buffer (β-catenin). After cooling, samples were placed in 3% H_2O_2 for 10 minutes to quench endogenous peroxide activity. After washing with PBS, slides were blocked with Super Block (ScyTek Laboratories, AAA500) for 10 minutes. The primary antibodies were incubated at the following concentrations in antibody diluent (PBS + 1% bovine serum albumin and 0.1% Tween 20): PanCK (Dako, Z0622; 1:200) and β-catenin (Abcam, ab32572; 1:100) for 1 hour at room temperature or at 4°C overnight. Samples were washed with PBS 3 times and incubated with the appropriate biotinylated secondary antibody (Vector Laboratories) diluted 1:500 in antibody diluent for 30 minutes at room temperature. Samples were washed with PBS 3 times and sensitized with the Vectastain ABC kit (Vector Laboratories, PK-6101) for 30 minutes. After 3 washes with PBS, color was developed with DAB Peroxidase Substrate Kit (Vector Laboratories, SK-4100), followed by quenching in distilled water for 5 minutes. Slides were counterstained with hematoxylin (Thermo Fisher Scientific, 7211) and dehydrated to xylene, and coverslips applied with Cytoseal XYL (Thermo Fisher Scientific, 8312-4). Images were taken on a Zeiss Axioskop 40 inverted microscope. Images for tiling were taken on a Zeiss Axio Observer.Z1 microscope and assembled with ZEN Imaging software.

Cell Quantification in Mice

To quantify the number of BEC-derived hepatocytes in mice, liver samples were stained for β-catenin, CK19, and HNF4A. For each sample, 5 images were taken with ×200 magnification, and the total number of $CK19^-/\beta\text{-catenin}^+/HNF4A^+$ cells in the image was counted in a blinded fashion. To quantify the levels of ductular reactions, $panCK^+$ area was measured using ImageJ. To quantify proliferation, the number of $\beta\text{-catenin}^+/HNF4A^+/PCNA^+$ cells was manually counted using the ImageJ cell counter program.

Western Blotting

To extract proteins, whole liver tissue was homogenized in radioimmunoprecipitation assay buffer as previously described.[9] Protein was separated on precast 4%–20% or 7.5% polyacrylamide gels (Bio-Rad) and transferred to a nitrocellulose membrane using the Trans-Blot Turbo Transfer System (Bio-Rad). Membranes were blocked for 90 minutes with 5% skim milk (LabScientific, M0841) and incubated with primary antibodies at 4°C overnight at the following concentrations: β-catenin (BD Biosciences, 610154; 1:1000), H3K9ac, (Abcam, ab4729; 1:10,000), H3K27ac (Millipore, 06-942, 1:5000), Histone H3 (Cell Signaling Technology, CS971; 1: 500,000), SOX9 (Abcam, ab5535; 1:1000), HDAC1 (Cell Signaling Technology, CS34859; 1:1000), and GAPDH (Santa Cruz, sc-25778; 1:1000). Membranes were washed in Blotto buffer and incubated with the appropriate horseradish peroxidase–conjugated secondary antibody for 2 hours at room temperature. Membranes were washed with Blotto buffer, and bands were developed with SuperSignal West Pico Chemiluminescent Substrate (Thermo Fisher Scientific, #34080) and visualized by autoradiography.

Human Studies

Fifteen cirrhotic liver tissue specimens were collected in Beijing You'an Hospital, Capital Medical University. Among them, 3 were HBV-associated compensated cirrhosis, 6 decompensated cirrhosis (4 with HBV infection and 2 with alcoholic hepatitis), and 6 were ACLF (3 with HBV infection and 3 with alcoholic hepatitis). The tissue specimens of compensated cirrhotic patients were obtained through liver biopsy, whereas large liver tissues were collected when decompensated cirrhotic and ACLF patients received liver transplantation. The study protocol was approved by the Ethics Committees of Beijing You'an Hospital, Capital Medical University. Written informed consent was obtained from patients or their representatives. For immunohistochemistry, liver tissues were fixed in 4% formaldehyde and embedded in paraffin for 4-μm sectioning. The slides were deparaffinized in xylene and rehydrated in a dilution series of graded ethanol to distilled water. Antigen retrieval was performed by microwave treatment in EDTA buffer (1 mmol/L, pH 8.0) for 10 minutes. The slides were incubated with 3% H_2O_2 for 30 minutes at room temperature. After washing with PBS 3 times, slides were incubated with primary antibodies against SOX9 (Sigma-Aldrich, HPA001758; 1:100) or HDAC1 (Santa Cruz Biotechnology, Sc-81598; 1:50) at 4°C overnight. The next day, the slides were washed with PBS 3 times, followed by incubating with EnVision peroxidase-labeled secondary antibodies (Dako) for 1 hour at room temperature. Peroxidase activity was detected with diaminobenzidine. The slides were counterstained with hematoxylin. Immunoreactivity was visualized under light microscopy.

References

1. Westerfield M. The zebrafish book: a guide for the laboratory use of zebrafish (*Danio rerio*). University of Oregon Press, 2000.
2. Takeuchi M, Fuse Y, Watanabe M, et al. LSD1/KDM1A promotes hematopoietic commitment of hemangioblasts through downregulation of Etv2. Proc Natl Acad Sci U S A 2015;112:13922–13927.
3. **Alexander J, Stainier DY**, Yelon D. Screening mosaic F1 females for mutations affecting zebrafish heart induction and patterning. Dev Genet 1998;22:288–299.
4. Choi TY, Khaliq M, Ko S, et al. Hepatocyte-specific ablation in zebrafish to study biliary-driven liver regeneration. J Vis Exp 2015:e52785.
5. **Shin D, Shin CH**, Tucker J, et al. Bmp and Fgf signaling are essential for liver specification in zebrafish. Development 2007;134:2041–2050.
6. de Groh ED, Swanhart LM, Cosentino CC, et al. Inhibition of histone deacetylase expands the renal progenitor cell population. J Am Soc Nephrol 2010;21:794–802.
7. **Ko S, Choi TY**, Russell JO, et al. Bromodomain and extraterminal (BET) proteins regulate biliary-driven liver regeneration. J Hepatol 2016;64:316–325.
8. Whittle N, Schmuckermair C, Gunduz Cinar O, et al. Deep brain stimulation, histone deacetylase inhibitors and glutamatergic drugs rescue resistance to fear extinction in a genetic mouse model. Neuropharmacology 2013;64:414–423.
9. Tan X, Behari J, Cieply B, et al. Conditional deletion of beta-catenin reveals its role in liver growth and regeneration. Gastroenterology 2006;131:1561–1572.
10. **Choi TY, Khaliq M**, Tsurusaki S, et al. Bone morphogenetic protein signaling governs biliary-driven liver regeneration in zebrafish through Tbx2b and Id2a. Hepatology 2017;66:1616–1630.
11. Ninov N, Borius M, Stainier DYR. Different levels of Notch signaling regulate quiescence, renewal and differentiation in pancreatic endocrine progenitors. Development 2012;139:1557–1567.
12. Cheung ID, Bagnat M, Ma TP, et al. Regulation of intrahepatic biliary duct morphogenesis by Claudin 15-like b. Dev Biol 2012;361:68–78.
13. Choi TY, Ninov N, Stainier DY, et al. Extensive conversion of hepatic biliary epithelial cells to hepatocytes after near total loss of hepatocytes in zebrafish. Gastroenterology 2014;146:776–788.
14. Wang Y, Pan L, Moens CB, et al. Notch3 establishes brain vascular integrity by regulating pericyte number. Development 2014;141:307–317.
15. Nambiar RM, Ignatius MS, Henion PD. Zebrafish colgate/hdac1 functions in the non-canonical Wnt pathway during axial extension and in Wnt-independent branchiomotor neuron migration. Mech Dev 2007;124:682–698.
16. **Delous M, Yin C**, Shin D, et al. Sox9b is a key regulator of pancreaticobiliary ductal system development. PLoS Genet 2012;8:e1002754.
17. Snyder JL, Kearns CA, Appel B. Fbxw7 regulates Notch to control specification of neural precursors for oligodendrocyte fate. Neural Dev 2012;7:15.
18. **Alunni A, Krecsmarik M**, Bosco A, et al. Notch3 signaling gates cell cycle entry and limits neural stem cell amplification in the adult pallium. Development 2013;140:3335–3347.

Author names in bold designate shared co-first authorship.

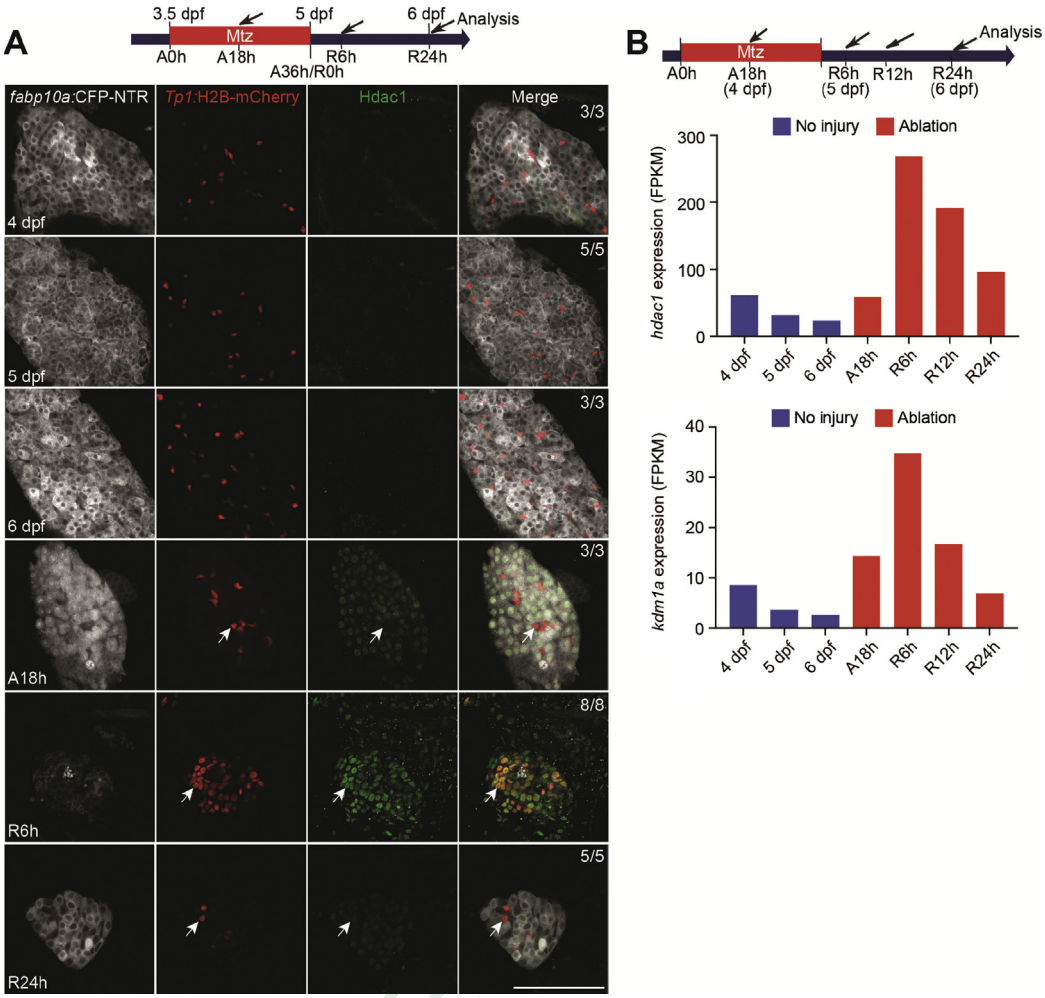

web 4C/FPO

Supplementary Figure 1. *hdac1* and *kdm1a* are highly up-regulated during BEC-driven liver regeneration. (*A*) Single-optical section images showing the expression of *fabp10a:*CFP-NTR (*grey*), *Tp1:*H2B-mCherry (*red*), and Hdac1 (*green*) in uninjured or regenerating livers. White arrows point to BECs. Scale bar, 100 μm. (*B*) Graphs showing the expression levels of *hdac1* and *kdm1a* among uninjured and regenerating livers at designated time points. These data were generated using the previously described RNA sequencing results.[10] FPKM, for fragments per kilo base of exon per million fragments mapped.

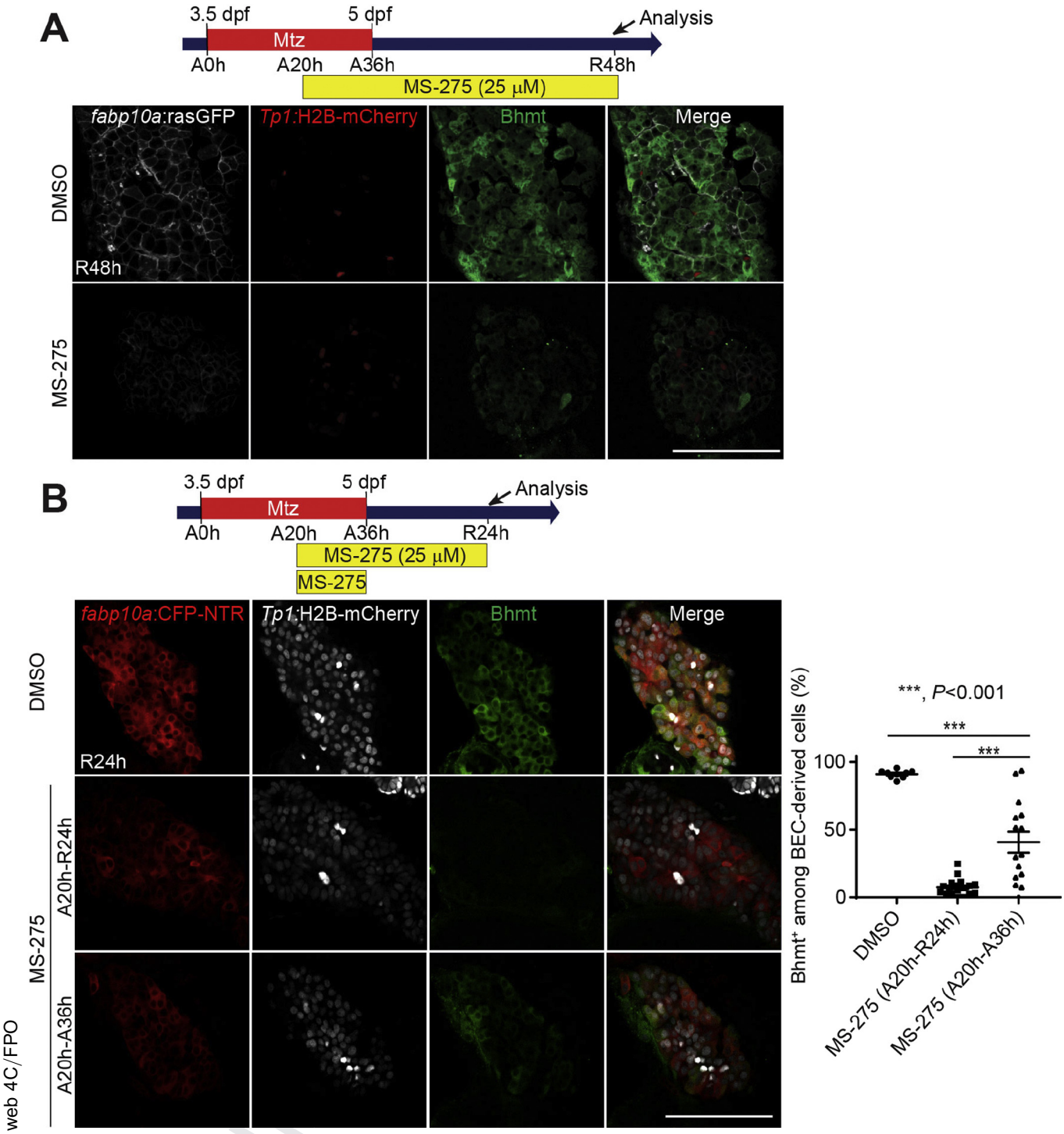

Supplementary Figure 2. The continuous treatment of MS-275 impairs LPC-to-hepatocyte differentiation during regeneration. (*A*) Single-optical section images showing the expression of Bhmt (*green*), *fabp10a:*rasGFP (*gray*), and *Tp1:*H2B-mCherry (*red*) in regenerating livers at R48h. (*B*) Single-optical section images showing the expression of Bhmt (*green*), *fabp10a:*CFP-NTR (red), and *Tp1:*H2B-mCherry (*gray*) in regenerating livers at R24h. Quantification of the percentage of Bhmt$^+$ hepatocytes among BEC-derived cells is shown. Scale bars, 100 μm; error bars show $\pm$ standard error of the mean.

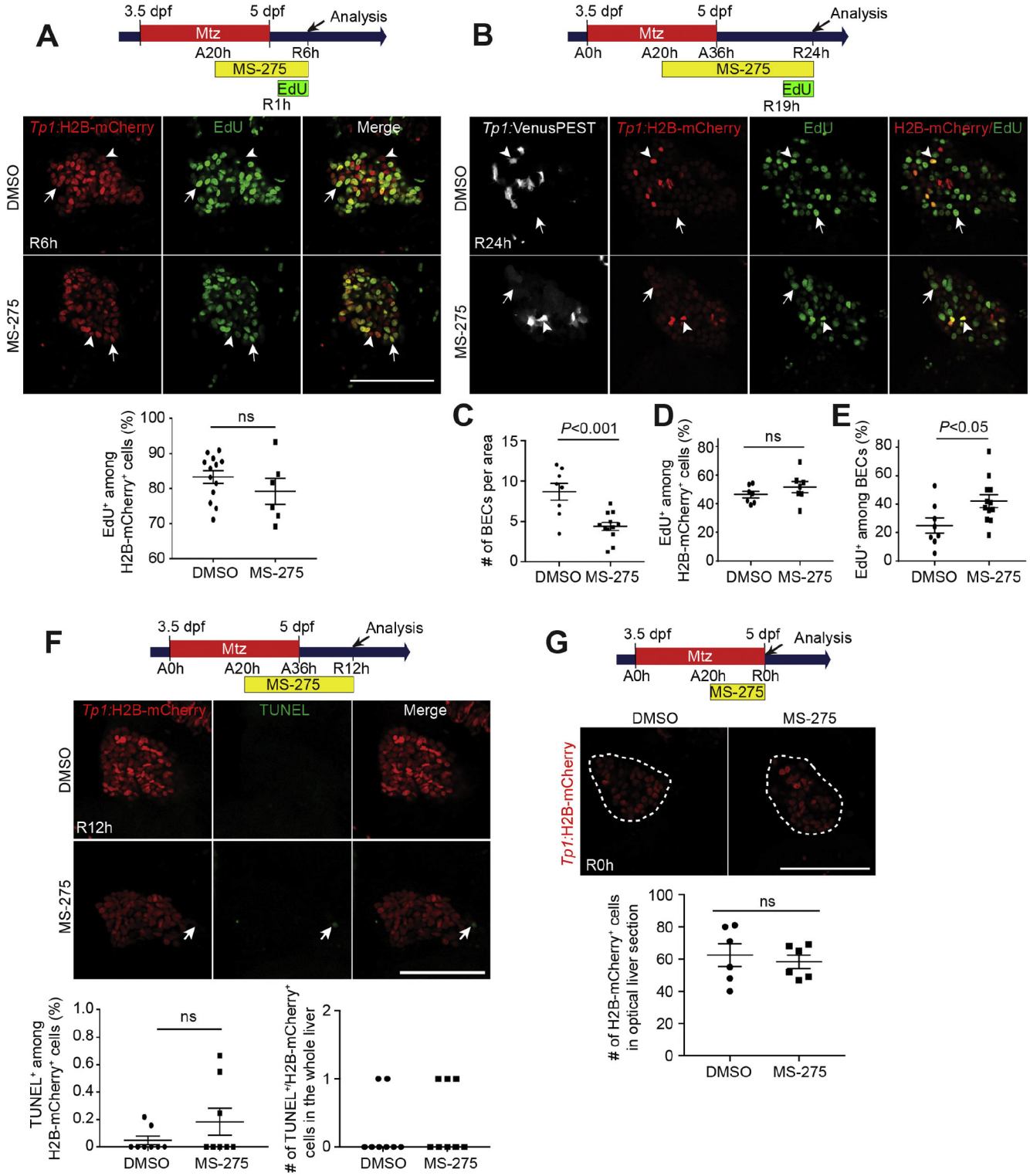
A
3.5 dpf
5 dpf
Analysis
Mtz
A20h
R6h
MS-275
EdU
R1h
Tp1:H2B-mCherry
EdU
Merge
DMSO
MS-275
R6h
EdU+ among H2B-mCherry+ cells (%)
ns
DMSO
MS-275
B
3.5 dpf
5 dpf
Analysis
Mtz
A0h
A20h
A36h
R24h
MS-275
EdU
R19h
Tp1:VenusPEST
Tp1:H2B-mCherry
EdU
H2B-mCherry/EdU
DMSO
MS-275
R24h
C
# of BECs per area
P<0.001
DMSO
MS-275
D
EdU+ among H2B-mCherry+ cells (%)
ns
DMSO
MS-275
E
EdU+ among BECs (%)
P<0.05
DMSO
MS-275
F
3.5 dpf
5 dpf
Analysis
Mtz
A0h
A20h
A36h
R12h
MS-275
Tp1:H2B-mCherry
TUNEL
Merge
DMSO
MS-275
R12h
TUNEL+ among H2B-mCherry+ cells (%)
ns
DMSO
MS-275
# of TUNEL+/H2B-mCherry+ cells in the whole liver
DMSO
MS-275
G
3.5 dpf
5 dpf
Analysis
Mtz
A0h
A20h
R0h
MS-275
DMSO
MS-275
Tp1:H2B-mCherry
R0h
# of H2B-mCherry+ cells in optical liver section
ns
DMSO
MS-275

web 4C/FPO

Supplementary Figure 3. The effect of MS-275 treatment on the proliferation and cell death of BEC-derived cells during BEC-driven liver regeneration. (*A*) Single-optical section images showing *Tp1:*H2B-mCherry expression (*red*) and EdU labeling (*green*) in regenerating livers at R6h. EdU was treated for 5 hours from R1h. Arrows point to EdU/H2B-mCherry double-positive cells; arrowheads point to H2B-mCherry single-positive cells. Quantification of the percentage of EdU$^+$ cells among H2B-mCherry$^+$ cells is shown. (*B*) Single-optical section images showing *Tp1:*H2B-mCherry (*red*) and *Tp1:*VenusPEST (*gray*) expression and EdU labeling (*green*) in regenerating livers at R24h. EdU was treated for 5 hours from R19h. Arrowheads point to EdU-positive BECs; arrows point to EdU-positive non-BECs. (*C*) Quantification of BEC number per area, as shown in *B*. (*D*) Quantification of the percentage of EdU$^+$ cells among H2B-mCherry$^+$ cells, as shown in *B*. (*E*) Quantification of the percentage of EdU$^+$ cells among BECs, as shown in *B*. (*F*) Confocal projection images showing *Tp1:*H2B-mCherry expression (*red*) and TUNEL labeling (*green*) in regenerating livers at R12h. Arrows point to TUNEL-positive, BEC-derived cells. Quantification of the percentage of TUNEL$^+$ cells among H2B-mCherry$^+$ cells is shown. Quantification of the total number of TUNEL$^+$ BEC-derived cells in the whole liver is also shown. (*G*) Single-optical section images showing *Tp1:*H2B-mCherry expression in regenerating livers (*dashed lines*) at R0h. Quantification of the number of *Tp1:*H2B-mCherry$^+$ BEC-derived cells is shown. Scale bars, 100 μm; error bars show $\pm$ standard error of the mean. ns, not significant.

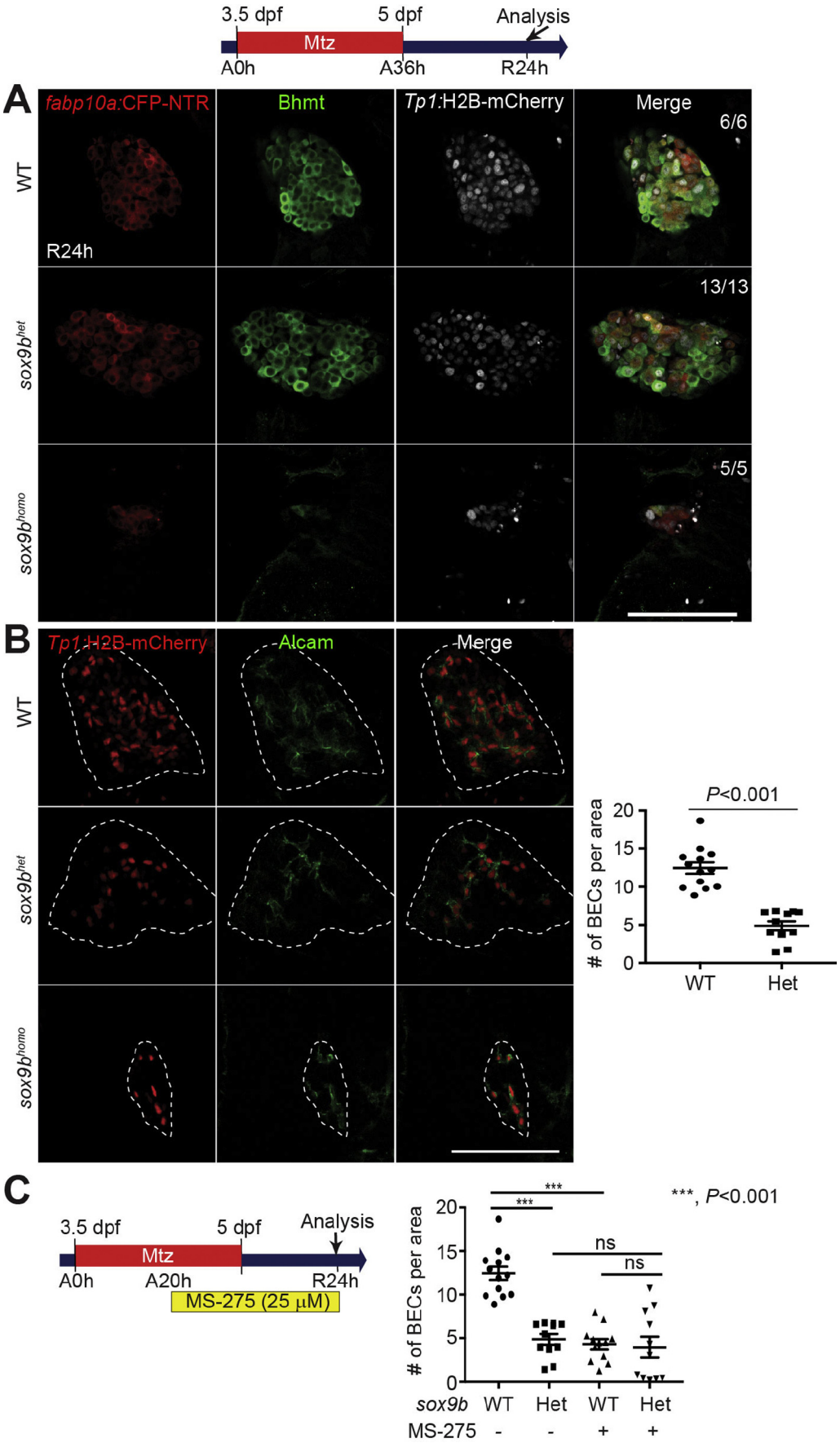
3.5 dpf
5 dpf
Analysis
Mtz
A0h
A36h
R24h
A
fabp10a:CFP-NTR
Bhmt
Tp1:H2B-mCherry
Merge
WT
R24h
6/6
sox9b^het
13/13
sox9b^homo
5/5
B
Tp1:H2B-mCherry
Alcam
Merge
WT
sox9b^het
sox9b^homo
P<0.001
# of BECs per area
20
15
10
5
0
WT
Het
C
3.5 dpf
5 dpf
Analysis
Mtz
A0h
A20h
R24h
MS-275 (25 μM)
***
***
ns
ns
***, P<0.001
# of BECs per area
20
15
10
5
0
sox9b WT Het WT Het
MS-275 - - + +

web 4C/FPO

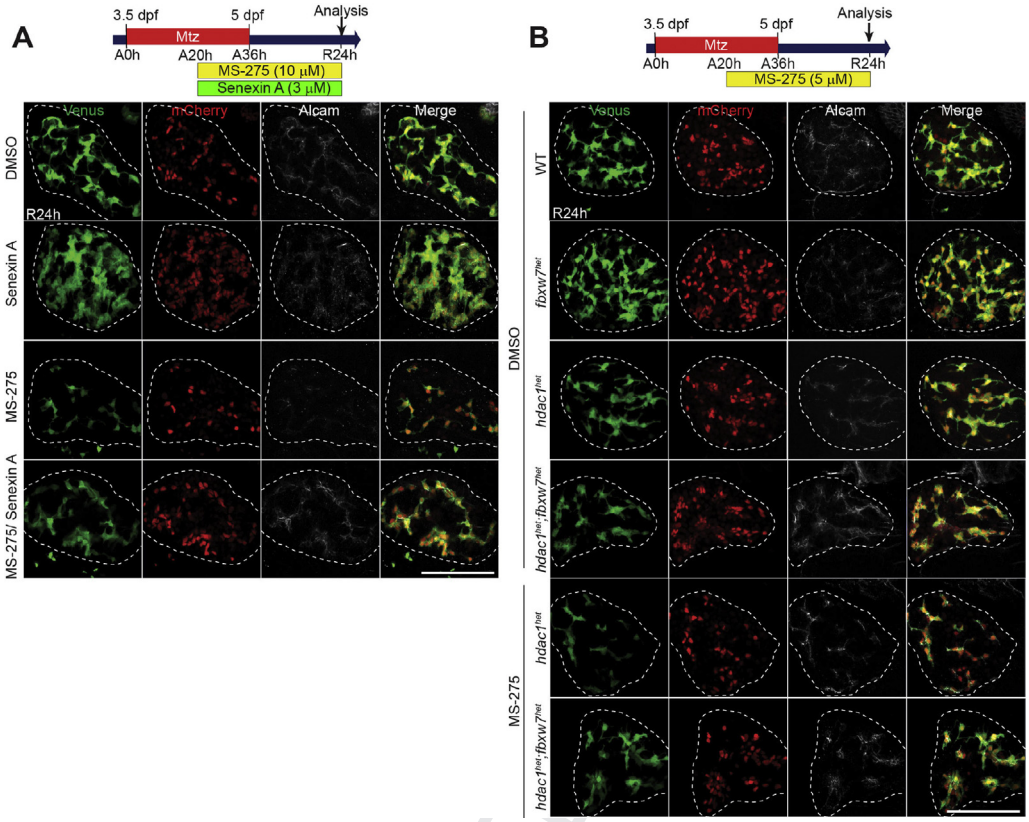

Supplementary Figure 5. Hdac1 regulates LPC-to-BEC differentiation via Cdk8 and Fbxw7. (*A*, *B*) Confocal projection images showing the expression of Alcam (*gray*), *Tp1:*VenusPEST (*green*), and *Tp1:*H2B-mCherry (*red*) in regenerating livers at R24h. Dashed lines outline regenerating livers. Scale bars, 100 μm. M, mol/L; WT, wild type.

web 4C/FPO

Supplementary Figure 4. BEC-driven liver regeneration in *sox9b* mutants. (*A*) Single-optical section images showing the expression of Bhmt (*red*), *fabp10a:*CFP-NTR (*red*), and *Tp1:*H2B-mCherry (*gray*) in regenerating livers at R24h. Numbers indicate the proportion of larvae exhibiting the representative expression shown. (*B*) Confocal projection images showing Alcam (*green*) and *Tp1:*H2B-mCherry (*red*) expression in regenerating livers at R24h. Dashed lines outline regenerating livers. Quantification of BEC number per area is shown. (*C*) Quantification of BEC number per area in regenerating livers at R24h. Scale bars, 100 μm; error bars show $\pm$ standard error of the mean. het, heterogeneous; M, mol/L; ns, not significant; WT, wild type.

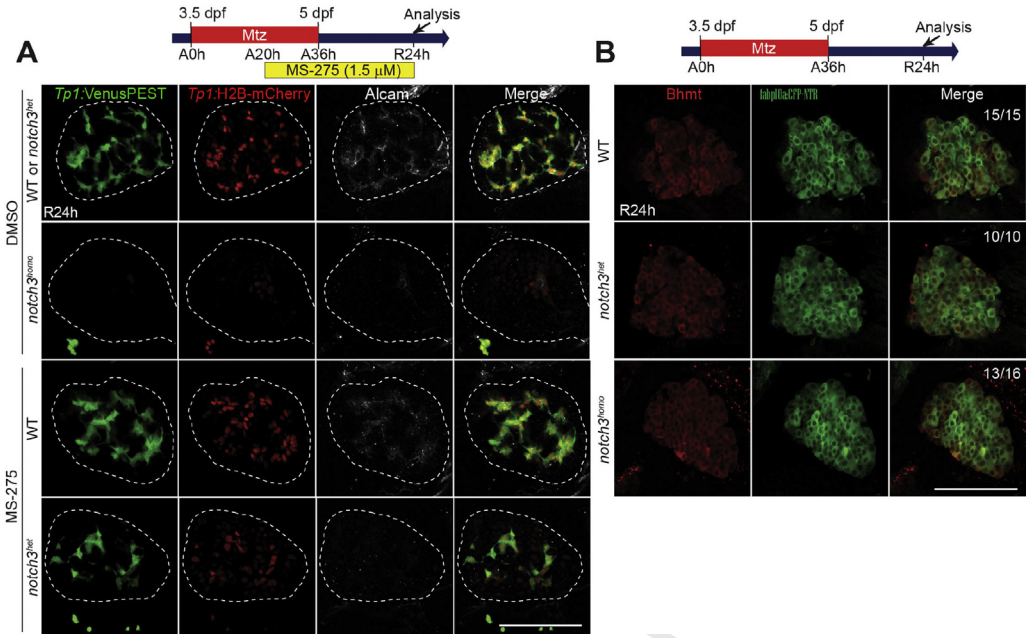

Supplementary Figure 6. BEC-driven liver regeneration in *notch3* mutants. (*A*) Confocal projection images showing the expression of Alcam (*gray*), *Tp1:*VenusPEST (*green*), and *Tp1:*H2B-mCherry (*red*) in regenerating livers (*dashed lines*) at R24h. (*B*) Single-optical section images showing Bhmt (*red*) and *fabp10a:*CFP-NTR (*green*) expression in regenerating livers at R24h. Numbers indicate the proportion of larvae exhibiting the representative expression shown. Scale bars, 100 μm. M, mol/L; WT, wild type.

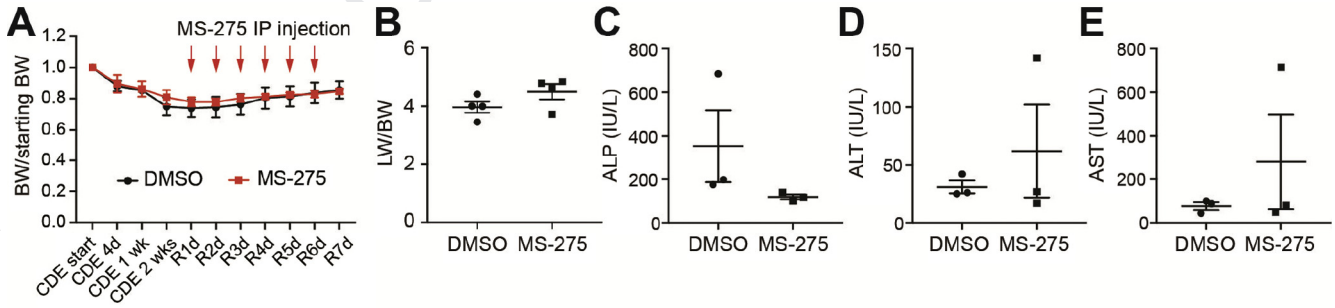

Supplementary Figure 7. MS-275 administration does not exacerbate liver damage in the KO mice fed a CDE diet. (*A*) Graph showing the tracking of body weight (normalized with starting body weight) during the entire experimental procedure. (*B–E*) Graphs showing (*B*) liver weight/body weight ratio and the serum levels of (*C*) alkaline phosphatase (ALP), (*D*) alanine aminotransferase (ALT), and (*E*) aspartate aminotransferase (AST) between DMSO- and MS-275–injected regenerating livers at R7d. BW, body weight; IP, intraperitoneal; LW, liver weight.

Supplementary Table 1. Transgenic and Mutant Zebrafish Lines Used in This Study

Names Used in This Study	Official Names (ZFIN Database)	Allele No.	Reference
Tg(Tp1:VenusPEST)	*Tg(EPV.Tp1-Mmu.Hbb:Venus-Mmu.Odc1)*	s940	11
Tg(Tp1:H2B-mCherry)	*Tg(EPV.Tp1-Mmu.Hbb:hist2h2l-mCherry)*	s939	11
Tg(fabp10a:rasGFP)	*Tg(-2.8fabp10a:CAAX-EGFP)*	s942	12
Tg(fabp10a:CFP-NTR)	*Tg(fabp10a:CFP-NTR)*	s931	13
Tg(hs:N3ICD)	*Tg(hsp70l:canotch3-EGFP)*	co17	14
hdac1	*hdac1*	b382	15
sox9b	*sox9b*	fh313	16
fbxw7	*fbxw7*	vu56	17
notch3	*notch3*	fh332	18
kdm1a	*kdm1a*	it627	2

Supplementary Table 2. List of Compounds Used for Chemical Screening

Chemical	Pathway	Concentration (μmol/L)
Phthalazinone pyrazole	Aurora A kinase inhibitor	30
Gemcitabine	GADD45A inhibitor	30
CPTH2	GCN5 inhibitor	3
UNC0224	G9A inhibitor	30
3-Deazaneplanocin A	EZH2 inhibitor	3
AMI-1	PRMT inhibitor	20
UNC1999	EZH2 inhibitor	20
Chaetocin	HMT inhibitor	20
Sirtinol	SIRT1/2 inhibitor	25
F-amidine	PAD4 inhibitor	15
WDR5-0103	WDR5 inhibitor	15
PD 173074	FGF R2-5 inhibitor	15
IOX1	2OG oxygenase inhibitor	25
Lomeguatrib	MGMT inhibitor	25
Tenovin-6	p53 activator	5
UNC1215	L3MBTL3 inhibitor	25
trans-Resveratrol	COX-1 inhibitor	25
DMOG	HIF-PH inhibitor	1
ZM 447439	Aurora B kinase inhibitor	25
C646	p300 inhibitor	0.5
I-CBP112	CBP/EP30 inhibitor	100
Sinefungin	SET domain-containing methyltransferase inhibitor	30
GSK-J4	JMJD3 inhibitor	50
Mirin	MRN inhibitor	100
BSI-201	PARP1 inhibitor	5
Ellagic acid	CARM1 inhibitor	30
(−)-Neplanocin A	SAH hydrolase inhibitor	30
PFI-3	SMARCA inhibitor	30
TSA	Pan HDAC inhibitor	0.5
MS-275	Class1 HDAC inhibitor	25
5-Azacytidine	DNMT inhibitor	100
OG-L002[a]	KDM1a inhibitor	100
Mdivi[a]	DNM1 inhibitor	100
Bafilomycin A1[a]	Autophagy inhibitor	0.01
LY294002[a]	PI3K inhibitor	40
U0126[a]	MEK inhibitor	100
XAV939[a]	WNT inhibitor	1
LG100754[a]	RXR inhibitor	5
GW501516[a]	PPARδ activator	3
AG1478[a]	EGF receptor inhibitor	1
Calcitriol[a]	VDR activator	5

[a]Not included in the epigenetic compound library.

Supplementary Table 3. Sequences of Primers Used for In Situ Probe Synthesis

Gene	Primer	Nucleotide sequence (5′ to 3′)
hdac1	forward	TGAGTCCTATGAAGCCATATTCAA
hdac1	reverse	CTTCTCCATCCTTCTCTTCTTCAG
kdm1a	forward	TGTACACTATGCCACGCCAG
kdm1a	reverse	TAATACGACTCACTATAGGGATGGGTTGGGTAGGCAGTTG
fbxw7	forward	GGCCCAGAGGTTCGATCTTT
fbxw7	reverse	TAATACGACTCACTATAGGGAAGGACTGTGTGTGAACCCC
cdk8	forward	CGGCATCCACTATTTGCACG
cdk8	reverse	TAATACGACTCACTATAGGGGCGGATTGGGTCCATGGTAA
skp1	forward	CCGACCATTAAACTGCAGAGC
skp1	reverse	TAATACGACTCACTATAGGGTGATCATGTTCGCAACCGTC

NOTE. Underlining indicates T7 primer sequences.

Supplementary Table 4. Sequences of Primers Used for qPCR

Gene	Primer	Nucleotide Sequence (5′ to 3′)
eef1a1l1	forward	CTGGAGGCCAGCTCAAACAT
eef1a1l1	reverse	ATCAAGAAGAGTAGTACCGCTAGCATTAC
hdac1	forward	AGGGGAGGATTGTCCTGTCT
hdac1	reverse	CCTTGCCTGCACCAATATCT
kdm1a	forward	TCATACTCGTACGTCGCAGC
kdm1a	reverse	TCCCAGGAACTGATCGGCTA
fabp10a	forward	GCAGGTTTACGCTCAGGAGA
fabp10a	reverse	TCCTGATCATGGTGGTTCCT
hnf4a	forward	GCCGACACTACAGAGCATCA
hnf4a	reverse	TGGTAGGTTGAGGGATGGAG
bhmt	forward	CTGATCGCTGAGTACTTTG
bhmt	reverse	CAATGAAGCCCTGGCAGC
sox9b	forward	CAGAAACACCCGACTCCAG
sox9b	reverse	CACACCGGCAGATCTGTTT
foxa1	forward	CACAAGAGGTCTATTCTCCCA
foxa1	reverse	GGACATGCCCATGTAACTG
foxa2	forward	AGAGCCTGAGTGTTACACC
foxa2	reverse	GACATAGTCATGTAAGTGTTCATGG
foxa3	forward	TGAAATTCCGGAGTGGAATC
foxa3	reverse	GCTGGGATAGCCCATATTCA
epcam	forward	CTTGTTTGTTGTGGCATTGG
epcam	reverse	TTGACGCACCAGCATACTTC
prox1	forward	AGCTTTTCCGTGCTCTCAAC
prox1	reverse	GGCATTGAAAAACTCCCGTA
fbxw7	forward	GGCCCAGAGGTTCGATCTTT
fbxw7	reverse	AAGGACTGTGTGTGAACCCC
skp1	forward	CCGACCATTAAACTGCAGAGC
skp1	reverse	TGATCATGTTCGCAACCGTC
cdk8	forward	CGGCATCCACTATTTGCACG
cdk8	reverse	GCGGATTGGGTCCATGGTAA
her9	forward	AATGCCAGCGAGCATAGAAAGTC
her9	reverse	TGCCCAAGGCTCTCGTTGATTC
her2	forward	AGCAATGGCACCAACTGTCTGC
her2	reverse	CCACCACCGGTTTCCTCAGTTTAG
her15.1	forward	AACGTCTCCAGCAAGAAGCTCAG
her15.1	reverse	TGCTTGATGTGTGTGTGCTGCTG

Supplementary Table 5. Sequences of Primers Used for ChIP-qPCR

Site	Primer	Nucleotide Sequence (5′ to 3′)
#1	forward	AAGAATGCTGGACGCCTGTT
#1	reverse	GGAATGTTGGAAAGCGGTCAC
#4	forward	GCTGCCATTGAGCAGTGTTT
#4	reverse	GCTGGCTTCCACACTCATCT
Control	forward	GCTTGCAGAACAACATGCAAC
Control	reverse	CAACGCATGAGGAAAGCCAT

Supplementary Table 6. Expression of SOX9 and HDAC1 in Patient Livers With Advanced Liver Diseases

	Cirrhosis	Decompensated cirrhosis		ACLF	
Protein	HBV (n = 3)	HBV (n = 4)	Alcohol (n = 2)	HBV (n = 3)	Alcohol (n = 3)
SOX9	3	4	2	3	3
HDAC1	3	4	0	0	0